Redox Geochemistry of the Late Cambrian SPICE Event in Durness Group, UK

Ke Feng[1], Rachel Wood[1*], Ferd Bowyer[1]

[1]*School of GeoSciences, University of Edinburgh, James Hutton Road, Edinburgh EH9 3FE, UK*

*Corresponding author. E-mail: rachel.wood@ed.ac.uk.

Keywords: “SPICE” event; marine redox; primary productivity; trilobite extinction; Fe speciation; I/(Ca+Mg)

Abstract

The Late Cambrian Steptoean Positive Carbon Isotope Excursion (SPICE) event occurring at approximately 497 Ma and lasting for about 2-4 Myr is emblematic of a global-scale

oceanic anoxia, coinciding with the trilobite mass extinction. It is significant in the biotic evolution spanning the Late Cambrian to Ordovician. Nevertheless, the driving mechanism behind the SPICE event is contentious, and its relationship with the trilobite mass extinction remains open. Therefore, to address these controversies and uncertainties, this study combined carbon and oxygen isotope analyses of the SPICE event in the Durness Group, with a comprehensive array of redox proxies, including I/(Ca+Mg) ratios, Fe speciation, TOC, and redox-sensitive trace elements, to elucidate the process of Durness SPICE event and provide insights.

Based on the sedimentological and geochemical characteristics of the Durness SPICE event, it can be delineated into five distinct stages corresponding to the transgressive-regressive cycles within the Sauk Megasequence. Stage I represents the pre-SPICE period of the Lower Systems Tract (LST). The $\delta^{13}C$ baseline hovers around -1‰, and Mo-U covariation signals a semi-restricted environment. Low Al (mean 0.16 wt%) and Ti (mean 205 ppm) contents suggest minimal terrestrial input. The I/(Ca+Mg) ratios (mean 0.23) signify suboxic conditions, with TOC (mean 0.016 wt%) maintaining baseline values; Phase II marks the onset of the SPICE event in transgressive system tract (TST) with rising sea level. $\delta^{13}C$ (mean 0.71‰) initiates an upward trend and Mo-U covariation shifts from semi-restricted to open conditions. Elevated Al (mean 0.67 wt%) and Ti (mean 432 ppm) concentrations point to increased terrigenous input. The TOC (mean 0.022 wt%) and I/(Ca+Mg) ratios (mean 0.25) briefly increase, returning subsequently to baseline, signifying heightened marine primary productivity that led to transient oxygenation and then progressed towards oxygen depletion. The $\delta^{13}C$ peaks (2.8‰) during the Maximum Flooding Surface (MSF), leading into Phase III, characterized by a gradual sea-level drop, representing the Highstand Systems Tract (HST) and subsequent Falling-Stage Systems Tract (FSST). $\delta^{13}C$ (mean 0.09‰) gradually returns to the baseline. The I/(Ca+Mg) ratio (mean 0.22) continues to decrease, and TOC (mean 0.016 wt%) remains at the baseline, confirming the intensification of suboxic conditions; Phase IV signifies a rapid regression,

where the Mo-U covariance indicates a more restricted environment, and Al (mean 0.96 wt%) and Ti (mean 495 ppm) concentrations further increase, signifying enhanced terrigenous input. Simultaneously, TOC (mean 0.03 wt%) and the I/(Ca+Mg) ratios (mean 0.22) rise, signalling transient oxygenation associated with a renewed increase in marine primary productivity, causing a slight rise in $\delta^{13}C$ (-0.31‰). A significant increase in U enrichment factors (EF) (mean 14.8) indicates a shift from suboxic to anoxic conditions; Phase V, the post-SPICE phase, corresponds to the Transgressive System Tract (TST) with rising sea levels. The Mo-U covariance indicates an open marine environment, while $\delta^{13}C$ (mean -0.97‰) and TOC (0.017 wt%) remain at baseline. The declining I/(Ca+Mg) ratios (mean 0.19) signify increased anoxia, with a single Mo EF (103) suggesting potential localized euxinia. Additionally, Fe_{HR}/Fe_T (mean 0.68) and Fe_{py}/Fe_{HR} (0.03) ratios suggest that after oxidation in Stage II, the Durness SPICE event primarily occurred under ferruginous conditions.

Through analyses of carbon isotopes, TOC, and comprehensive redox proxies, it is demonstrated that multiple eustatic fluctuations initiated the SPICE event, supporting the theory of anoxia resulting from increased nutrient input-driven marine primary productivity, thereby transitioning shallow tidal flats from suboxic to anoxic environments. Furthermore, it further elucidates the collaborative controls of deep nutrient-rich upwelling and enhanced continental weathering on the SPICE event, as well as the diffusion of deep basin euxinia to shallow shelves and the influence of palaeolatitude on weathering patterns, resulting in distinct local expressions of the global SPICE event at varying palaeolatitudes. This provides novel insights into the SPICE event. Moreover, the oxidation during the initial stages of the SPICE event challenges the hypothesis of widespread deep anoxia-driven trilobite extinction, favouring a scenario where rising sea levels led to increased marine primary productivity, disrupting the food chain, and triggering the trilobite mass extinction. Additionally, it introduces a potential driving force behind the significant and sustained increase in atmospheric oxygen levels during the post-SPICE period, which is

the widespread ferruginous environment during the SPICE event. This enhances our understanding of the relationship between the SPICE event and the Great Ordovician Biodiversification Event occurring approximately 30-40 Myr later.

1. Introduction

Throughout Earth's evolutionary history, the pervasive issue of inadequate oxygen in the oceans has been posited as a principal causative factor for biotic extinctions. Recent sedimentary geochemical investigations have revealed that, in the Late Cambrian, atmospheric oxygen content had attained notably elevated levels (Saltzman et al., 2011; Berner, 2001, 2006; Beerling et al., 2002). Nevertheless, the paucity of oxygen was evident within the oceanic milieu (Fig. 1C), exerting a substantial influence on biological evolution (Gill et al., 2011; Hough et al., 2006; Hurtgen et al., 2009). Although the Early Cambrian heralded the advent of myriad biological phyla during the Cambrian Explosion (Gould, 1989) (Fig. 1A), the Middle to Late Cambrian witnessed a succession of recurrent biotic mass extinctions (Servais et al., 2009, 2010; Harper, 2006; Sepkoski, 1981), this may be attributed to environmental volatility, which is concretely manifested in the rapid oscillations between positive and negative excursions in carbon isotope within palaeo-oceans (Brasier et al., 1994) (Fig. 1B). Consequently, alterations in carbon isotope serve as proxies for elucidating the Cambrian environmental and climatic evolution, rendering carbon isotope excursion patterns an imperative avenue of research in Cambrian palaeontology, palaeoecology and palaeoclimatology.

The study of the global carbon cycle holds paramount significance in the investigation of climate and marine redox changes. Carbon isotopes, archived within carbonate rocks, conventionally serve as proxies for the isotopic composition of dissolved carbon in seawater. Consequently, the examination of carbon isotopic trends within carbonate rocks

facilitates the elucidation of prolonged, large-scale excursions in global oceanic carbon isotope signatures. Across the entire geologic record, carbonate rocks have experienced recurrent and substantial fluctuations in carbon isotopic compositions. These conspicuous episodes of carbon isotopic anomalies commonly exhibit correlations with momentous geological or palaeobiological evolutionary events, as well as changes in stratigraphy and sea levels (Saltzman et al., 2011) (Fig. 1B). As a result, the comprehensive and interdisciplinary exploration of carbon isotopic anomalies within the geological record proves advantageous in providing a more holistic comprehension of the determinants governing the global carbon cycle and its implications for the course of biological evolution.

The Steptoean Positive Carbon Isotope Excursion (SPICE) event, occurring at the base of the Paibian stage of Furongian (Fig. 1B), stands as a notable global anoxic event within the late Cambrian. This event is a critical repository of geological insights regarding global climate changes and ranks among the foremost geological occurrences for the study of Cambrian and Ordovician palaeobiological evolution, climatic perturbations, and environmental alterations (e.g., Saltzman, 1998; Saltzman et al., 2000, 2011; Peng et al., 2004; Zhu et al., 2004; Gill et al., 2011; Kouchinsky et al., 2008; Sial et al., 2008; Chen et al., 2011, 2012). Diverse geochemical studies have been undertaken on the Furongian strata to scrutinize changes in the marine redox milieu and its potential connection to mass extinctions. Nonetheless, these topics, as well as the triggers of the SPICE event remain a subject of ongoing debate (e.g., Saltzman et al., 2011; Gill et al., 2011; Schiffbauer et al., 2017; Li et al., 2018). Therefore, conducting systematic investigations into representative Cambrian strata can offer robust geochemical substantiation for the exploration of the evolutionary trajectory of the redox environment during the SPICE event and its plausible associations with mass extinctions. Considering this, delving into the patterns of carbon isotope excursion within the Cambrian not only elucidates palaeoenvironmental transformations and climatic vicissitudes but also furnishes pivotal underpinnings for the

study of biological evolution, thus bearing profound theoretical and scientific import.

The carbonate sediments within Scotland comprise a segment of the vast Great American Carbonate Bank. In the northern reaches, the Durness Group exposes extensive Cambrian to Ordovician carbonate rock strata, offering invaluable insights for investigating palaeo-oceanic environments spanning the Cambrian to the Ordovician periods. The bottom of the Durness Group is marked by the Eilean Dubh Formation, which archives the occurrence of the SPICE event at the southern extremity of the Laurentia (Raine, 2010). However, the Durness SPICE event has, thus far, only been recorded in a study (Pruss et al., 2019), which primarily sought to assess the efficacy of mercury as a redox proxy within a Carbon Isotope Excursion (CIE) devoid of large igneous provinces, without addressing the Durness SPICE event problems. As such, this study plans to conduct systematical carbon isotope analyses on the data-sparse Durness SPICE event and integrate a comprehensive suite of redox proxies, encompassing Fe speciation, I/(Ca+Mg) ratio, and redox-sensitive elements such as molybdenum and uranium. The aim is to delve profoundly into the causation and mechanisms of the Durness SPICE event, as well as its correlation with the trilobite mass extinction and the Ordovician radiation, thus contributing to the study of global SPICE events and early Paleozoic biological evolution.

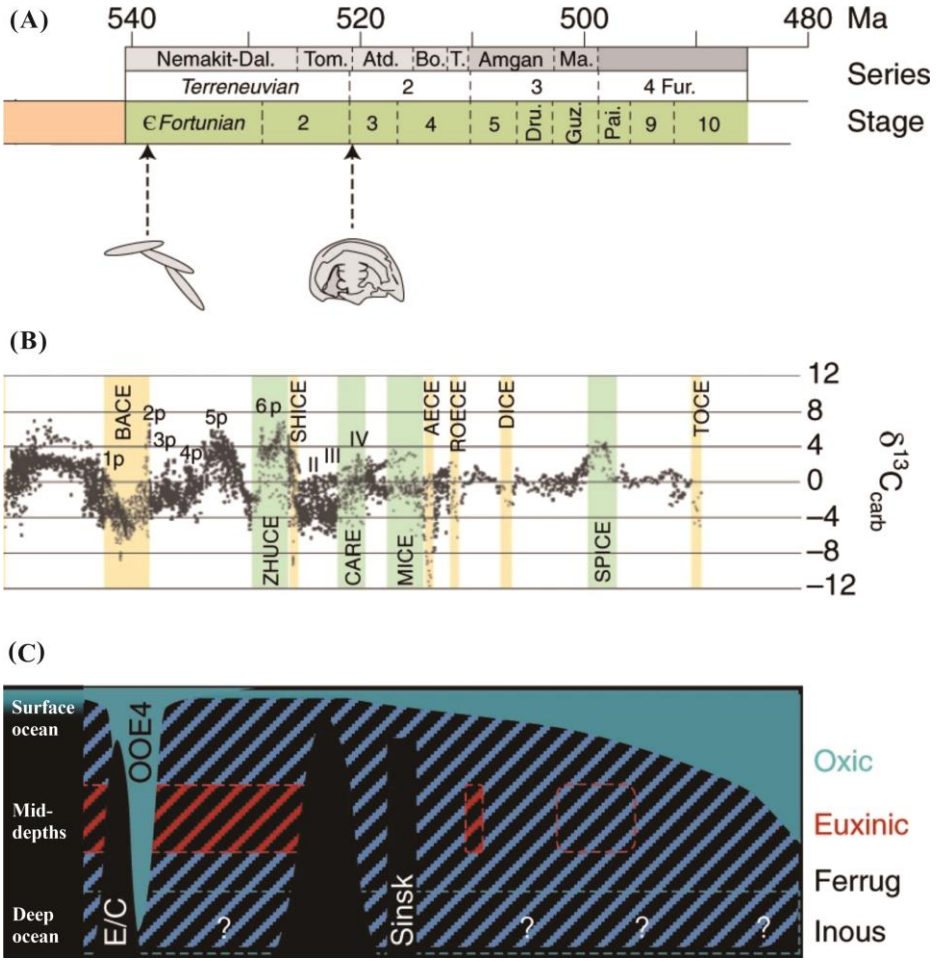

Fig.1 The Comprehensive Geochemical and Biological Records of the Cambrian Period (modified after Wood et al., 2019). (A) First occurrences of key evolutionary benchmarks during Cambrian (the initial appearance datum of trace fossil *Treptichnus pedum*; the earliest trilobite *Profallotaspis jakutensis*); (B) The Cambrian carbon isotope profiles conform to a composite curve (refer to section 1.2 for details); (C) Diagram depicting the evolution of Cambrian redox conditions based on Fe speciation data (E/C, Ediacaran–Cambrian; OOE, oceanic oxygenation event; white question marks, no data).

2. Geological setting

The Hebridean Terrane encompasses the portion of northwestern Scotland, situated west of the Moine Thrust Belt. It represents a fragment of the Laurentian Craton. The passive margin of Laurentian Terrane formed after the disintegration of the supercontinent Pannotia and the onset of rifting in the Iapetus Ocean around 600-580 Ma (Torsvik et al., 1996; Scotese, 2009). Recent research indicates a two-phase process in the formation of

the Iapetus Ocean between Gondwana and Laurentia around 570 Ma, followed by continued rifting between 540 Ma and 535 Ma, leading to the establishment of the Laurentian passive margin as a narrow rift (Cawood et al., 2001) (Fig. 12). A sequence of unmetamorphosed red arkosic sandstones and conglomerates (alluvial fans, rivers, and lakes) of the Middle to Early Neoproterozoic Sleat, Stoer, and Torridon groups unconformably overlay the Archaean and Palaeoproterozoic gneissic basement. Following the Late Neoproterozoic Rodinia rifting (Torsvik et al., 1996), these rocks were levelled, forming a broad and shallow marine shelf upon which a series of Cambrian-Ordovician rocks were deposited. The tectonic subsidence and sedimentation at the margin extended from the southeastern United States to Canada and Newfoundland, even reaching as far as northern Greenland, spanning distances of several thousand kilometers. The subsidence history and stratigraphic record of the Newfoundland-Scotland-East Greenland margin exhibit significant similarities (Swett & Smit, 1972; Wright & Knight, 1995; Higgins et al., 2001). The Durness Group carbonate rocks consistently overlie dominantly siliciclastic rocks and the late Cambrian rocks assigned to the Ardvreck Group (Fig. 13C).

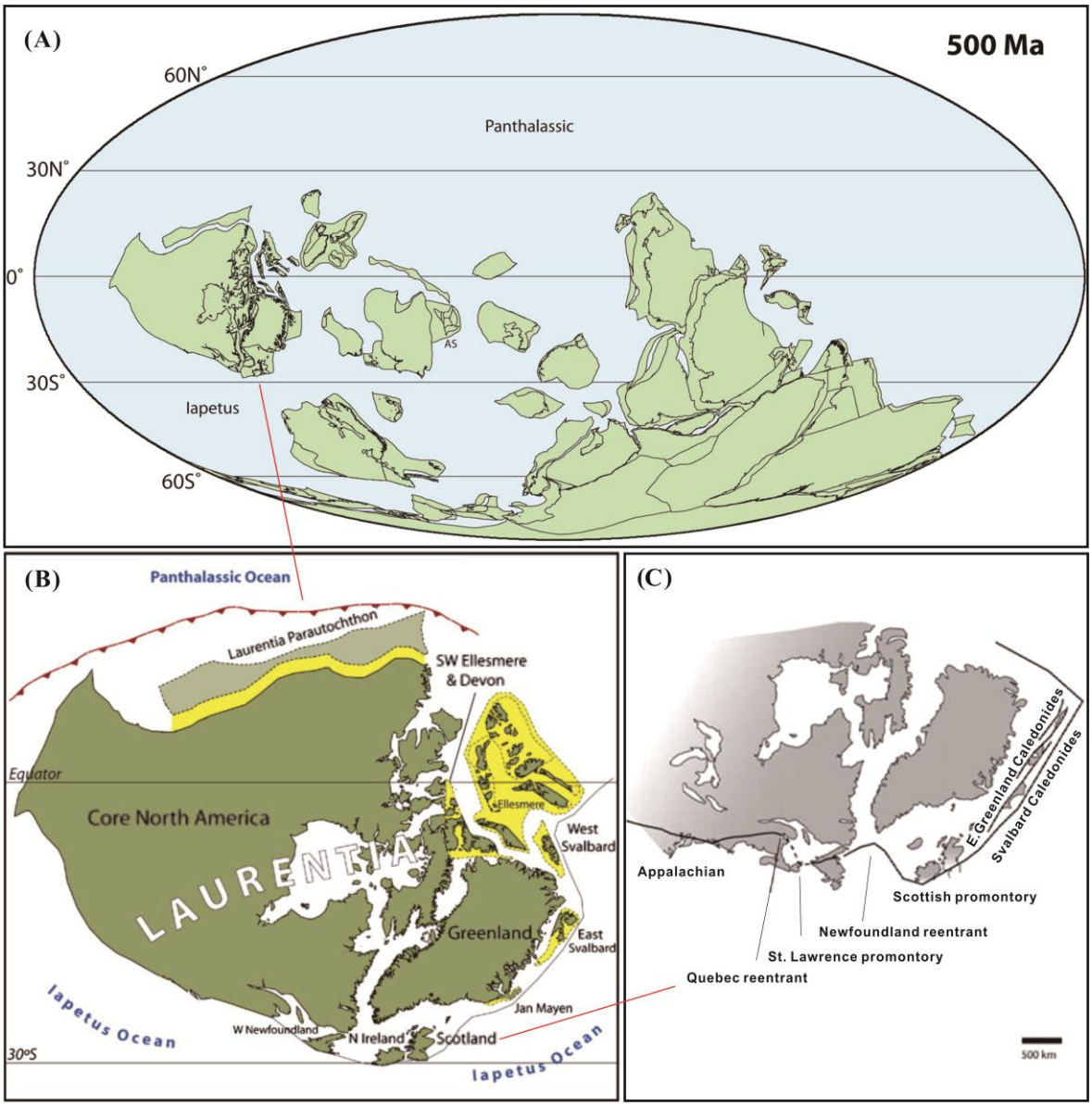

Fig. 12 (A) Palaeogeographic reconstruction of the Late Cambrian Furongian terranes (500Ma) (Torsvik and Cocks, 2013); (B) Late Cambrian Laurentia Palaeogeographic Map (the yellow shading represents potential continental areas and terrane extensions) (Cocks and Torsvik, 2011); (C) The Close-Up View of the Laurentian Margin, depicting the positions of Scotland and major promontories and re-entrants (modified after Cawood et al. 2007; Raine, 2010).

2.1 Durness Group

The Durness Group derives its name from the village of Durness in the northwest of Scotland. It comprises limestone and dolomite formations spanning peritidal and shallow subtidal environments of at least 920 meters thick, deposited along the passive margin of

the Iapetus Ocean known as the Laurentian margin (Raine, 2010). This rock assemblage is well-exposed in the vicinity of the Durness village. Lapworth (1883) referred to this rock sequence as the Durness or Eriboll Limestone, while Peach & Horne (1884) and Peach (1907) provided a more detailed characterization as the "Calcareous Series". Subsequently, Cowie et al. (1972) established the group status of the Durness Carbonates. These carbonates record sedimentation in tropical settings, comprising a succession of dolomite, limestone and dolomitic limestone transitioning from subtidally to supratidally sediments, interspersed with cherts and minor evaporite pseudomorphs. The group is replete with diverse microbialites, displaying a variety of stromatolites and thrombolites forms, with a localized abundance of ooids. This is congruent with existing palaeogeographic reconstructions placing Laurentia within the latitudinal range of approximately 30° N to 30° S during the Cambrian-Ordovician period (Cocks and Torsvik, 2006), with Scotland positioned at a palaeolatitude of around 30° S (Fig. 12A, B).

The rocks of the Cambrian-Ordovician are exposed in a narrow, nearly continuous belt, rarely exceeding 10 kilometers in width, extending southwestward for 180 kilometers from Loch Eriboll to Skye (Fig. 13A). The Durness Group outcrops to the west of the Moine Thrust Zone, with its eastern rocks being overlain by allochthonous metamorphic rocks of the Moine Supergroup. The Ardvreck Group and the lower two overlying formations of the Durness Group are widely exposed along the Moine Thrust Zone. A complete Durness Group (comprising 7 formations) is only found near Durness, with its upper boundary disrupted by a thrust fault. On Skye Island, all but the uppermost Durness Group is exposed, although continuous sections for detailed study are lacking. The type area of the Durness Group is the Durness Peninsula, with the most complete sections located at Balnakeil Bay, where the Eilean Dubh, Sailmhor, Sangomore, and Balnakeil formations are well-exposed (Fig. 13B). The lower boundary of the group coincides with the Salterella Grit Member, marked by a flooding surface. The upper boundary is truncated by thrust faults, as observed in Sango Bay.

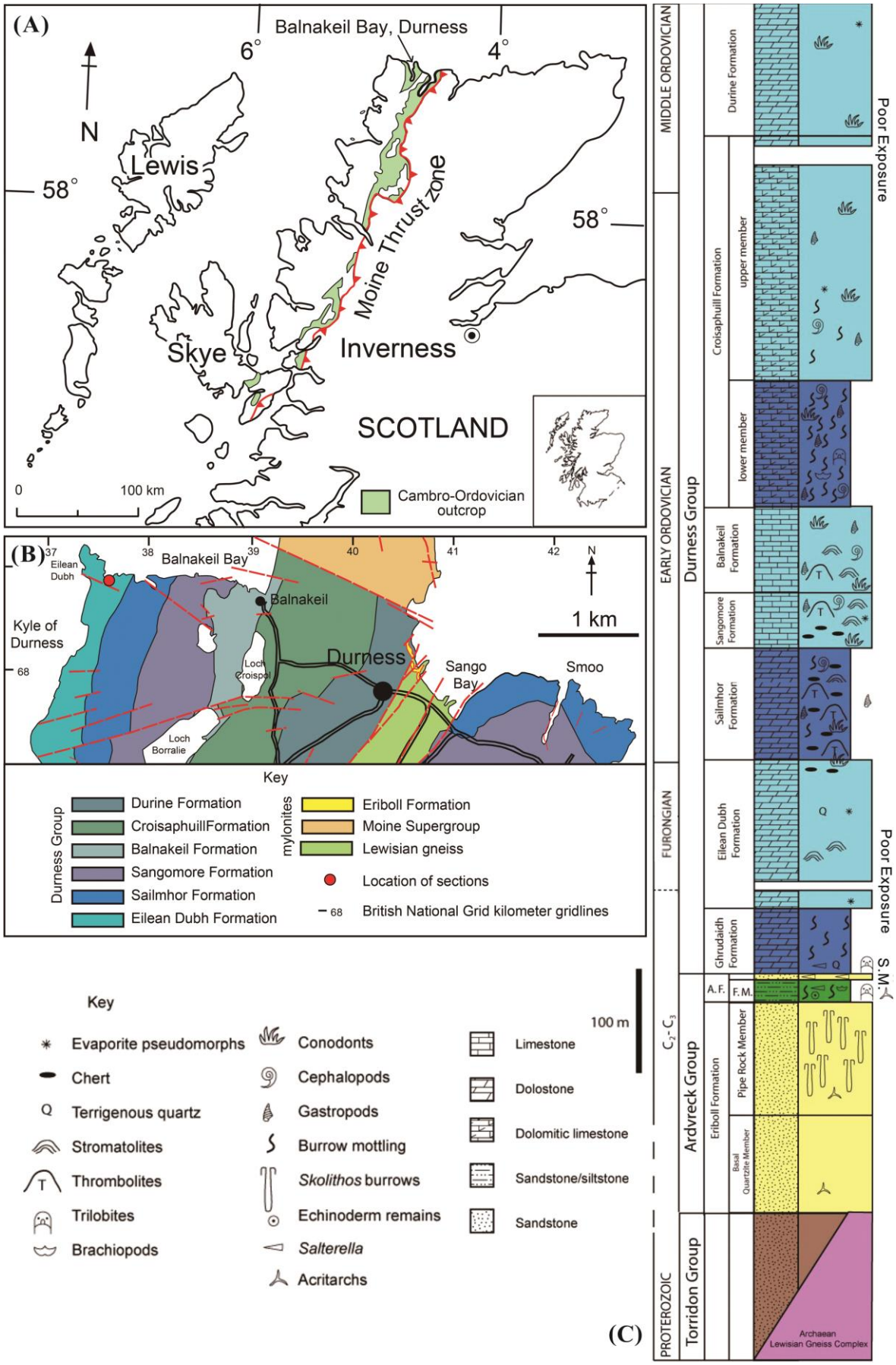
(A)
Balnakeil Bay, Durness
6°
4°
N
Lewis
58°
Moine Thrust zone
58°
Skye
Inverness
SCOTLAND
0
100 km
Cambro-Ordovician outcrop
(B)
37
38
Balnakeil Bay
39
40
41
42
N
Eilean Dubh
Balnakeil
1 km
Kyle of Durness
68
Loch Croispol
Durness
Sango Bay
Smoo
Loch Borralie
Key
Durness Group
Durine Formation
CroisaphuillFormation
Balnakeil Formation
Sangomore Formation
Sailmhor Formation
Eilean Dubh Formation
mylonites
Eriboll Formation
Moine Supergroup
Lewisian gneiss
Location of sections
68
British National Grid kilometer gridlines
MIDDLE ORDOVICIAN
EARLY ORDOVICIAN
FURONGIAN
PROTEROZOIC
Durness Group
Ardvreck Group
Torridon Group
Durine Formation
Croisaphuill Formation
upper member
lower member
Balnakeil Formation
Sangomore Formation
Sailmhor Formation
Eilean Dubh Formation
Ghrudaidh Formation
A.F.
F.M.
Eriboll Formation
Pipe Rock Member
Basal Quartzite Member
Archaean Lewisian Gneiss Complex
Poor Exposure
Poor Exposure
S.M.
Key
Evaporite pseudomorphs
Chert
Terrigenous quartz
Stromatolites
Thrombolites
Trilobites
Brachiopods
Conodonts
Cephalopods
Gastropods
Burrow mottling
Skolithos burrows
Echinoderm remains
Salterella
Acritarchs
100 m
Limestone
Dolostone
Dolomitic limestone
Sandstone/siltstone
Sandstone
(C)

Fig. 13 (A) The map illustrating the locations of the study area (Balnakeil Bay, Durness) about the Caledonian Main Thrust and the Cambrian-Ordovician outcrops (modified after Raine, 2009); (B) The map provides a detailed location depicting the geology, local settlements, and named landmarks (Raine and Smith, 2017); (C) Schematic Sedimentary Succession of the Cambrian-Ordovician Transition in Northwestern Scotland, depicting lithostratigraphy, lithology, and principal fossil groups. The An t-Sròn Formation is represented by A.F., the Fucoid Member by F.M., and the Salterella Grit Member by S.M (modified after Raine, 2009).

2.2 Eilean Dubh Formation

The target formation for recording the SPICE event is the Eilean Dubh Formation (Peach & Horne, 1884), named after the Eilean Dubh Peninsula located at the western end of Balnakeil Bay. Its type of section stretches along Balnakeil Bay. Exposures can also be observed in An t-Sròn and Stronchrubie, although they are significantly disrupted by intrusions. The formation is present on the Ord of Skye but is faulted against the upper boundary of the Sailmhor Formation. The lower boundary is seen in An t-Sròn and Grudie, where the transition from light grey and cream weathering dolomites to light grey, mottled, sucrosic, dark grey dolomites of the Ghrudaidh Formation (with some finer-grained, white dolomite layers in the upper part of the formation). The upper boundary is evident in Stronchrubie, Balnakeil Bay, and Kyle coastline, but it is faulted at Ord, Skye. Across all these locations, the boundary is essentially consistent.

Wright (1993) divided the unit into three members (Kyle, Stromatolite, and Solmar), but these three members are not fully defined, with the bases of the lower two members placed above the non-exposed parts. No similar partition was found in the Eilean Dubh Formation at Assynt. However, this could be due to numerous exposures of thrust faults and intense recrystallization. Owing to the complexity of structures, determining the thickness of the Eilean Dubh Formation in Assynt is challenging. Wright (1993) recognized the lower and upper parts of the Eilean Dubh rocks in the Assynt area but did not identify the stromatolite member. Approximately 121 meters have been measured in Balnakeil Bay, where the rocks include stromatolites fine-grained ripple laminated dolomites, mud-flake breccias, and

minor clastic sediments and evaporite pseudomorphs. The base of this formation is exposed for 12 meters in An t-Sròn, and differences with the lowest well-log profiles in Balnakeil Bay indicate no overlap, suggesting a minimum thickness of 133 meters for the formation (Fig. 13C).

2.3 Sedimentary background of Eilean Dubh Formation

The sedimentary facies of the Eilean Dubh Formation exhibited common sedimentary structures typical of peritidal sedimentation: mudcracks, ripples, tepees, and planar stromatolites, also including pseudomorphs of nodular and bedded anhydrite, vugs from dissolution of sulfate crystals, and halite casts, all of which supported the interpretation of a sabkha sedimentary environment, and the continental shelf was basically restricted (Raine, 2010). Additionally, throughout the studied section, siltstones and sandstones were intermittently observed, primarily composed of siliciclastic material. These siliciclastic sediments were likely transported onto the continental shelf through eolian processes, appearing as cycle caps, or they could represent the base of the next cycle after undergoing successive marine transgression (Raine and Smith, 2017).

At the base of the Eilean Dubh Formation, there are laminated dolomites rich in evaporites and stromatolites. Approximately 20 meters into the sequence, the evaporites diminish, and a minor influx of quartz sand becomes evident. Around 50 meters, quartz sand content increases, reaching its peak at 60-65 meters, accompanied by abundant stromatolites, evaporites, and teepee structures. Beyond 65 meters, both quartz sand and evaporites exhibit signs of decline. The lithology of the Eilean Dubh Formation distinctly reflects eustatic changes.

The Eilean Dubh Formation has been confirmed to correspond to the Sauk Megasequence, which is interpreted as representing deposition subsequent to progressive flooding of the Laurentian Craton during an extended period of rising sea level (Morgan, 2012). It was

further subdivided into three smaller-scale (second order) transgressive-regressive cycles or supersequences (Sauk I-III), each separated by eustatic lowering of sea levels (Palmer and Taylor, 1981).

Based on sea-level variations, Raine and Smith (2017) positioned the lower 20 meters of the Eilean Dubh Formation within the Sauk IIA Supersequence. Abundant evaporites in this interval indicate a lowstand systems tract (LST) associated with a lowering of sea level. Subsequently, as sea levels rose, the influx of quartz sand occurred from approximately 20 meters to about 63 meters, marking the range of the Sauk IIB Supersequence. It is divided by the Maximum Flooding Surface (MSF) and the regressive surface of marine erosion (RSME) into three parts: the transgressive systems tract (TST) in the lower part (20-35 m), characterized by laminated dolomites, the middle highstand systems tract (HST) (35-50 m), and the falling-stage systems tract (FSST) in the upper part where stromatolites, evaporites, and ripple lamination began to develop (50-63 m). At 60-65 meters, a crucial Sauk II–III Supersequence Boundary was identified, signifying a rapid and brief shallowing of sea level, followed by extensive flooding and a subsequent rapid sea-level rise (Raine and Smith, 2017). The Sauk II–III Supersequence Boundary was recognized worldwide by the regression and influx of abundant siliciclastic sediments, and it was no exception within the Eilean Dubh formation. Following the Sauk II–III Supersequence Boundary, the strata represent the Sauk IIIA Supersequence. Evidence of evaporites gradually decreases, indicating a rise in sea level and marking the transgressive systems tract (TST) (Fig. 14).

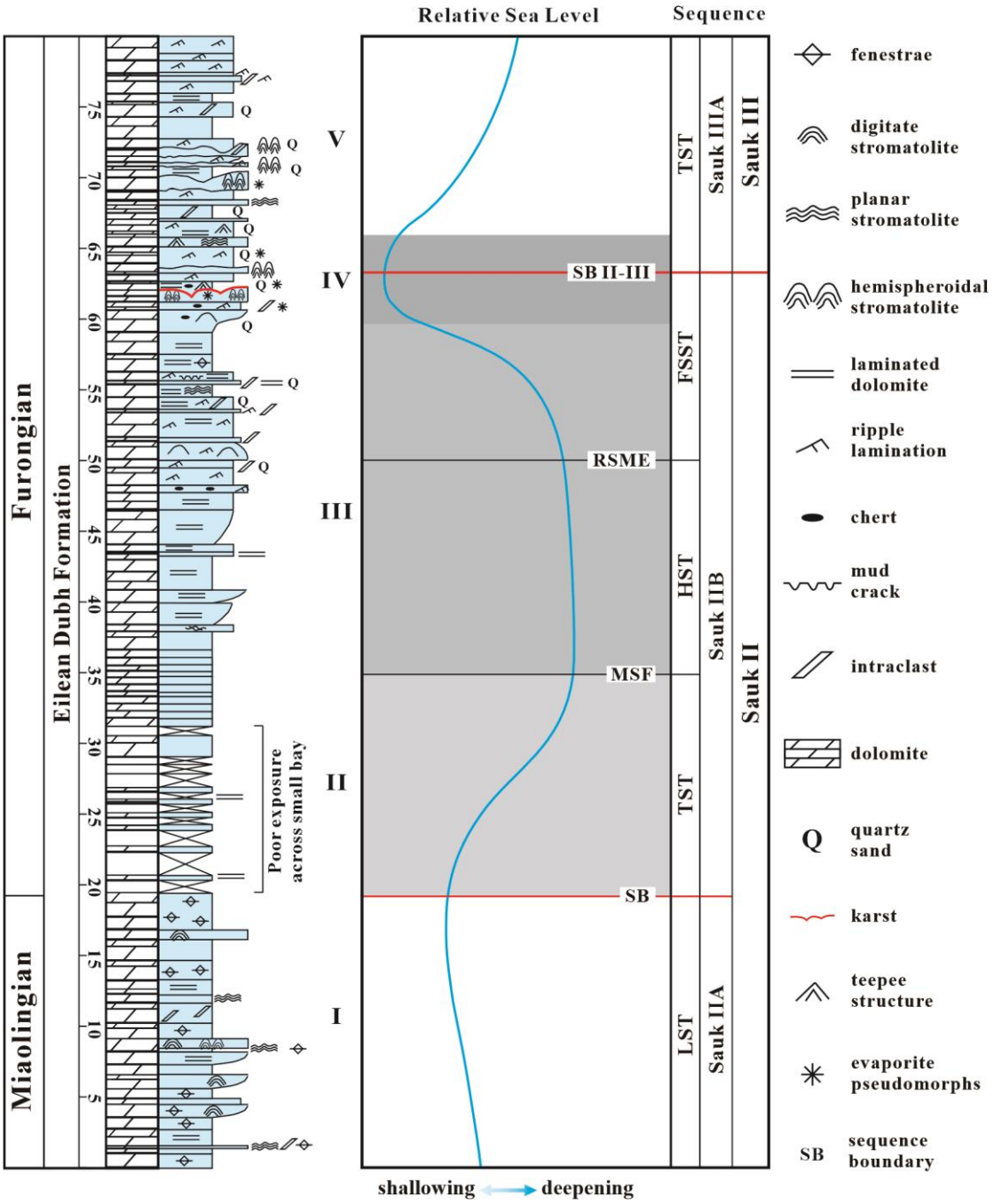

Fig. 14 The lithological column (modified after Raine, 2009), and sea-level variations (modified after Raine and Smith, 2017) of the Eilean Dubh Formation, along with its sequence stratigraphy systems tract divisions and their corresponding positions within the Sauk Megasequence (modified after Raine and Smith, 2012). The division into five stages is discussed in detail in Section 5.1.

3. Methods

In the field outcrop of the Eilean Dubh Formation, Upper Cambrian, located in northern Scotland, 77 samples were collected by Professor Rachel Wood and Andrew Curtis of carbonate rocks (dolomites) at meter-scale intervals. The samples spanned from the Late Cambrian Miaolingian to Furongian, to acquire geochemical information pertaining to the Durness SPICE event.

The bulk samples were cleaned, dried, and subsequently finely pulverized to a particle size finer than 100 mesh, facilitating various geochemical experiments, A total of five distinct analyses were performed, encompassing carbon and oxygen isotopes, elemental concentrations, total organic carbon (TOC), I/(Ca+Mg) ratios, and Fe speciation. The total digestion for elemental concentrations and the Fe speciation experiments were conducted at the Cohen Geochemistry Laboratory, University of Leeds. Concurrently, the assessments of I/(Ca+Mg) ratios and TOC content were undertaken at the University of Edinburgh. The carbon and oxygen isotope analyses were outsourced to Iso-Analytical for specialized processing.

3.1 Carbon and oxygen isotopes

For carbon and oxygen isotopic analysis, samples will be reacted with 99% H_3PO_4 at 75°C for 16 h using a stable isotope ratio mass spectrometer. The standard for the analysis is IAEA CO-8 Calcite. All results will be reported with reference to the Vienna Peedee Belemnite (VPDB) standard. The $\delta^{13}C$ values of the fluid are calculated using Golyshev's (1981) equilibrium carbon isotope fractionation equation ($103\ \ln\alpha_{dolomite\text{-}fluid} = 0.0758 \times 10^{18}\ T^{-6} - 5.767 \times 10^{12}\ T^{-4} + 31.3743 \times 10^{9}\ T^{-3} - 62.581 \times 10^{6}\ T^{-2} + 49.208 \times 10^{3}\ T^{-1} - 11.393$). The fluid's $\delta^{18}O$ values were determined by the equilibrium oxygen isotope fractionation equation ($103\ \ln\alpha_{dolomite\text{-}fluid} = 4.06 \times 10^{6}\ T^{-2} - 4.65 \times 10^{3}\ T^{-1} + 1.71$) (Zheng, 1999).

3.2 Elemental concentrations

80-90 mg of the samples were weighed and placed into crucibles, followed by heating at 500℃ for 24 hours to eliminate impurities. Subsequently, 5 ml of 5% nitric acid was added. After waiting for the reactions to reach equilibrium, hydrofluoric acid was introduced to achieve complete dissolution of the samples. The samples were then left to naturally air dry for 12 hours to ensure complete desiccation. Afterwards, the dried samples were dissolved in 5 ml of nitric acid at 80 degrees Celsius. Upon confirming the absence of solid residues, the samples were diluted with 18.2 MΩ cm deionised water (MQ) to a final volume of 100 ml. The total digestion solution comprised 4 ml of sample dilution, 5.9 ml of MQ, and 4.1 ml of internal standard. Subsequent elemental analysis was conducted using Inductively Coupled Plasma Optical Emission Spectrometer (ICP-OES) at the University of Leeds, aiming to determine the concentrations of major elements—Al and Fe—and trace elements—Ti, Mo, and U. The instrumental error did not exceed 3%.

3.3 TOC

Approximately 3 g of samples were roughly weighed and added to 10 ml of 10% hydrochloric acid for decarbonization. After allowing the reaction to settle, the mixtures were placed on a shaker for 12 hours, with continuous degassing to prevent leakage. Subsequently, centrifugation at 4000 rpm for 4 minutes was performed, followed by decanting the liquid and adding 10 ml of 10% hydrochloric acid for decarbonization again. This process was repeated 5 times until no reaction occurred upon the addition of hydrochloric acid. Then, 10 ml of ultrapure water was added and decanted the liquid after centrifugation. This rinsing procedure was repeated three times to remove residual impurities. Subsequently, the sample was placed in a drying oven at 40°C for 48 hours to ensure complete dehydration, thereby completing the decarbonization process. After this, 40-50 mg of the decarbonized sample was meticulously weighed and placed into a tin foil capsule, followed by folding and compacting. Finally, the TOC contents of samples were

analyzed using a Thermo FlashSmart Elemental Analyzer at the University of Edinburgh (RSDs % < 5 %).

3.4 I/(Ca+Mg) ratios

This approach was developed by Dr. Tianchen He from the University of Leeds and is consistent with the previously employed methodologies (Lu et al., 2010; Hardisty et al., 2014).

Approximately 10-20 mg of sample powders were roughly weighed and added 2 ml of ultrapure water. Subsequently, placed samples on a shaking table for 30 minutes, then centrifuged the tubes at 10,000 rpm for 1 minute, and decanted the liquid. This water addition and centrifugation process was repeated three times to ensure the thorough removal of clay minerals, dissolvable halogens, and salts. After this, the tubes were left open in a drying cabinet at 40 ℃ for 48 h to ensure complete desiccation. The dried samples were ground to finer and more homogenized powders using an agate mortar and then stored in aluminium foil envelopes to minimize the effect of static charge on weighing accuracy.

5-6 mg of the clean samples were meticulously weighed and introduced 1 ml of 3% nitric acid slowly, then placed samples in an ultrasonic bath until the reaction had fully subsided, and no gas bubbles were observed. Sealed and shook the tubes thoroughly and centrifuged at 10,000 rpm for 10 minutes. Subsequently, 0.5 ml of the supernatant was mixed with 0.5 ml of ammonium hydroxide to stabilize iodine, forming 1 ml mother solutions.

Combined 0.3 ml of the supernatant with 8.6 ml of 0.5% nitric acid and 0.1 ml of 10 ppb yttrium to create 9 ml solutions for the determination of calcium and magnesium concentrations using ICP-OES. The mother solutions were mixed with 0.5% nitric acid, 0.5% ammonium hydroxide, and 3% methanol, and diluted to solutions containing 50±5 μg/ml

of calcium and magnesium for subsequent ICP-MS analysis to obtain iodine values.

This method was repeatedly measured using the aragonite coral reference material JCp-1 to ensure long-term accuracy, yielding an I/(Ca+Mg) ratio precision of 4.013+/-0.036 μmol/mol (n=5). The I/(Ca+Mg) ratio obtained in this study was corrected based on the long-term value of 4.31 μmol/mol for JCp-1 from the University of Leeds facility. The detection limit for iodine was approximately 0.1 ppb (Lu et al., 2010, 2018). Analytical precision for all measured elements was better than 3%

3.5 Fe speciation

The Fe speciation method was developed by Poulton and Canfield, 2005, Canfield et al., 1986, as used by Zegeye et al., 2012, Goldberg et al., 2012, is divided into two sub-samples:

Sub-sample I: precisely measured 60-70 mg of the samples and mixed with 5 ml of 0.5 M hydrochloric acid. The mixtures were shaken for 1 hour to ensure a comprehensive extraction of carbonate-associated Fe (Fe_{carb}). After this, samples were centrifuged at 4000 rpm for 4 minutes and then collected 1 ml supernatant with 9 ml of 1% nitric acid to prepare Fe_{carb} solutions. For the second step, added 10 ml of 58.82 g/L sodium citrate, 20 ml/l acetic acid, and 50 g/L sodium dithionite mixture after decanted supernatant, and shook for 2 hours to thoroughly extract ferric (oxyhydr) oxides (Fe_{ox}), such as goethite and hematite. After another centrifugation step, 1 ml supernatant was collected, and combined with 9 ml of 1% nitric acid to prepare the Fe_{ox} solutions. The supernatant was once again decanted, followed by the addition of a 10 ml solution containing 28.42 g/L ammonium oxalate and 21.45 g/L oxalic acid to extract Magnetite (Fe_{mag}). The mixture was shaken for 6 hours, and the Fe_{mag} solution was prepared through repetitive procedures. The Fe contents in all Fe solutions were measured using atomic absorption spectrometry (AAS), ensuring an analytical precision of better than 3%.

Sub-sample II: Approximately 5 grams of the samples were weighed and treated with 8 ml of 50% hydrochloric acid. The mixture was boiled for 1 hour, and the evolved gases were passed into silver nitrate solutions to collect acid volatile sulfides (Fe_{AVS}). Following this, 15 ml of 1 M chromic chloride dissolved in 50% hydrochloric acid was added, and the boiling process continued for another hour. Sulfides were captured as silver sulfide by silver nitrate solutions. The precipitates were weighed, and the silver sulfides were quantitatively converted into pyrite concentrations through the stoichiometric method (Canfield et al., 1986, Fossing and Jørgensen, 1989), achieving an extraction precision of better than 5%.

4. Results

All the data for this study can be found in the appendix I and II.

Carbon Isotopes

The Durness Group SPICE carbon isotope curve was constructed from data from 38 samples. Its baseline hovers around -1‰, starting to rise at 10 m and peaking around 2.8 ‰ at 35 m. It then declines, returning to the baseline at 52 m, followed closely by a small positive excursion peaking around -0.03 ‰ at approximately 63 m, before returning to the baseline once again by 65 m (Fig. 15). This curve aligns perfectly with the carbon isotope curve recorded in previous SPICE studies in the Durness Group (Pruss et al., 2019, Fig. 11).

TOC

Comprising carbonate-rich dolomites, the Durness Group samples exhibit carbonate content of over 90%, resulting in low TOC concentrations for all 75 samples. The TOC curve begins near a baseline of approximately 0.02 wt%, rises at 20 m to a peak of 0.07 wt% at 25 m and subsequently settles near the baseline. An anomalous peak of around 0.09 appears at 64 m. Additionally, the TOC curve exhibits minor, regular fluctuations in proximity to the baseline, forming cycles of approximately 5 m (Fig. 15).

I/(Ca+Mg)

All 42 I/(Ca+Mg) values are significantly below 0.5. The I/(Ca+Mg) curve starts around 0.25, gradually decreases, then sharply rises at 20 m, peaking at 0.4 at 22 m, followed by fluctuations and returning to baseline at 39 m. A minor positive excursion peaks around 0.24 at 62 m before returning to baseline at 65 m. Overall, the I/(Ca+Mg) curve exhibits a gradual declining trend from 0.25 to 0.17 (Fig. 15).

Fe Speciation

The Fe speciation remains unaffected by lithology in the case of carbonate-rich samples with a total Fe concentration exceeding 0.5 wt% (Clarkson et al., 2214). Therefore, 22 samples were chosen to acquire Fe speciation data. The data starts at 25 m, and the ratios fluctuate and peak at 33 m (0.91), returning to baseline around 39 m. It continues a slow rise, with a minor dip at 62 m before returning to baseline. The Fe_{HR}/Fe_T ratios show an overall upward trend, increasing from 0.55 to 0.76. Another function of the Fe speciation is to distinguish ferruginous and euxinic environments through the extent of pyritization (Fe_{Py}) of the highly reactive Fe (Fe_{HR}) pool. All Fe_{Py}/Fe_{HR} ratios are significantly lower than 0.7, which is the threshold for potential euxinic conditions. Two anomalous peaks are observed: the first peak occurs at around 35 m, reaching 0.24, while the second is situated around 64 m, with a value of 0.06. The remaining Fe_{Py}/Fe_{HR} ratios hover around 0.03 (Fig. 15).

Elemental Concentrations

77 samples were analyzed for 2 major elements: Al and Fe, and 3 trace elements: Ti, Mo, and U. Some samples have elements below the limits of detection, resulting in missing data, e.g., aluminum in samples 12-15. Except for Mo and U, other elements display similar patterns. Samples from the initial 20 m exhibit markedly low element concentrations, while those beyond 20 m experience a sharp increase in element concentrations. Besides this, all elements exhibit a subsequent enrichment after about 60 m (Fig. 15).

Aluminium

The content of Aluminium displays extremely low levels in the initial 20m, with half samples below the limit of detection. It fluctuates between 0.02 - 2.8 wt%, and the average value for samples from the first 20 m was 0.16 wt%, while the range from 20 to 60 meters

exhibits an average of 0.72 wt%. From 61 to 79 meters, the average Al concentration rises to 1.07 wt%.

Titanium

Titanium exhibits characteristics closely resembling those of Aluminum. Its concentration in the first 20 meters is significantly low, with an average of 205 ppm. Beyond 20 meters, there is a sharp increase, with an average concentration of 476 ppm in the 20-60 m range. At depths of 60-79 meters, there is yet another pronounced enrichment, with concentrations reaching 509 ppm. Notably, the concentration curve for Titanium reveals the presence of a baseline at approximately 200 ppm.

Ferrum

Fe concentrations remain relatively consistent in the first 20 meters, with slight variations near an average of 0.21 wt%. Beyond 20 meters, Fe concentrations fluctuate irregularly, with an average of 0.65 wt% in the 20-60 m range and 0.93 wt% in the 60-79 m range. The minimum detectable Fe content for Fe speciation analysis is 0.5 wt%.

Molybdenum

The concentrations of Mo remain relatively stable in the first 20 meters and the 20-60 m range, with values of 0.54 ppm and 0.58 ppm, respectively. After 60 meters, there was a significant enrichment, with an average concentration of 1.21 ppm.

Uranium

Uranium shares a similar pattern with Mo, with an average concentration of 0.61 ppm in the first 20 meters, 0.68 ppm in the 20-60 m range, and a pronounced enrichment after 60 meters, with an average concentration of 1.97 ppm.

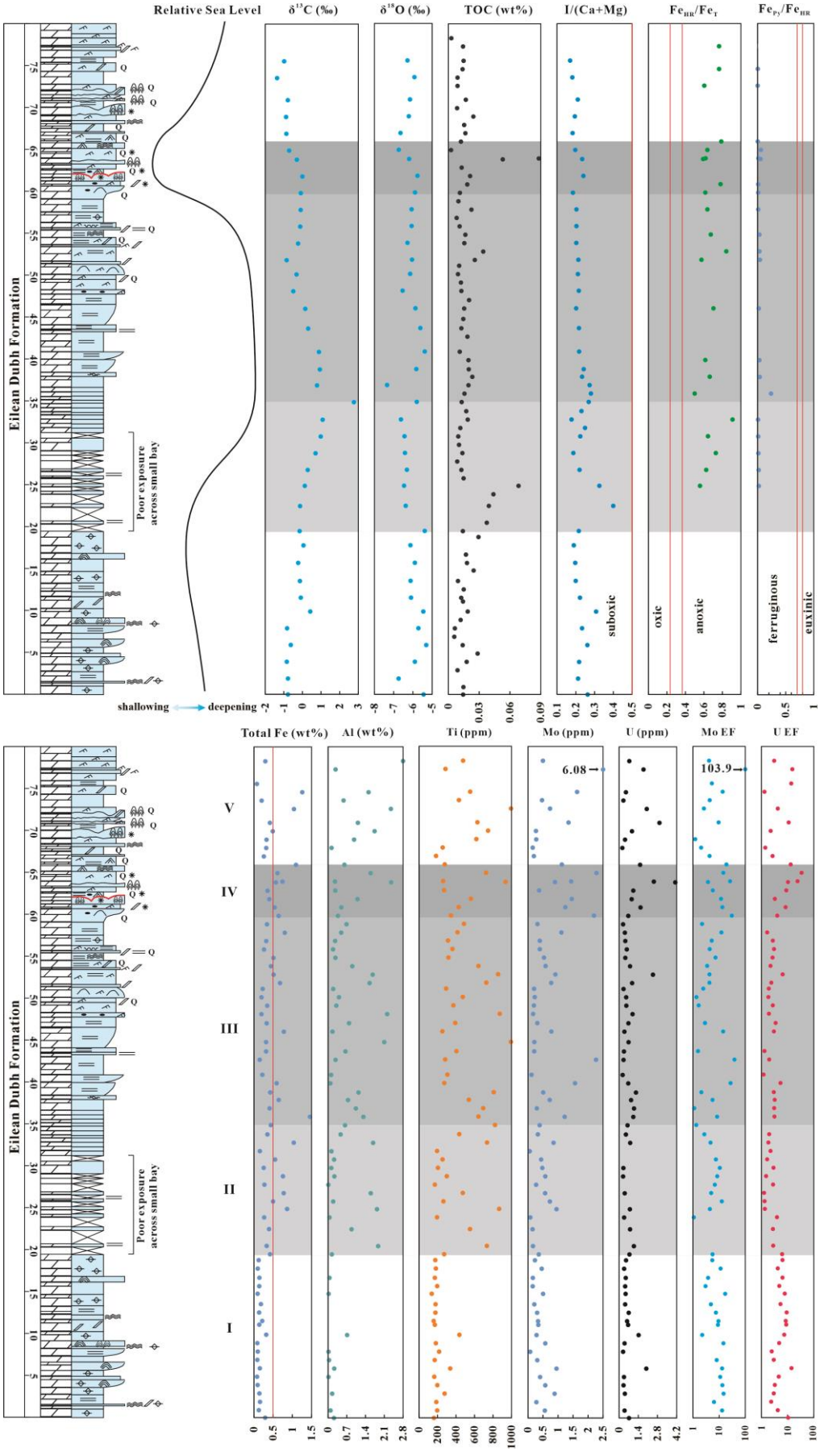
Eilean Dubh Formation
Poor exposure across small bay
Relative Sea Level
shallowing
deepening
δ13C (‰)
δ18O (‰)
TOC (wt%)
I/(Ca+Mg)
FeHR/FeT
FePy/FeHR
suboxic
oxic
anoxic
ferruginous
euxinic
Total Fe (wt%)
Al (wt%)
Ti (ppm)
Mo (ppm)
U (ppm)
Mo EF
U EF
6.08
103.9
I
II
III
IV
V

Fig. 15 The stratigraphic column of the Eilean Dubh Formation (modified after Raine, 2009), sea level variation (modified after Raine and Smith, 2012), and geochemical data curves. The division into five stages is discussed in detail in Section 5.1. The legend is shown in Figure 14.

This study plans to delineate the Durness SPICE event into distinct stages based on the unique characteristics observed in lithology, sedimentology, sequence stratigraphy, and geochemistry of Durness Group samples before commencing the discussion. Prior to conducting redox analysis, it is imperative to eliminate the influence of terrigenous material. This ensures that trace element proxies faithfully represent genuine redox fluctuations, allowing for the commencement of redox analysis.

5. Discussion

5.1 The classification of the Durness SPICE event progression

Based on the distinct characteristics observed in the Eilean Dubh Formation through data of carbon isotopes, I/(Ca+Mg) ratios, Fe speciation, and elemental concentrations, the study strata can be divided into three phases of significant changes and further subdivided into five stages (Fig. 14, 15).

The first phase spans from 0 to 20 m: (I) Before the onset of the SPICE event, major and trace elements have not yet begun to accumulate. TOC and the I/(Ca+Mg) ratios have not started to increase.

The second phase covers depths of 20 to 60 m, marks by the emergence of the SPICE event, signifying changing conditions. Diverse fluctuations manifest across all geochemical data: (II) Within the 20-35 m range, this stage spans from the initiation to the peak of the SPICE event. Carbon isotopes notably rise, and enrichment of major and trace elements commences. TOC, I/(Ca+Mg), and Fe_{HR}/Fe_T ratios exhibit a sharp ascent followed by a decline, indicating a turbulent stage; (III) Ranging from 35 to 60 m, this represents a relatively stable period following the peak of the SPICE event. Carbon isotopes start to regress, and the extent of major and trace element enrichment stabilizes, as do the curves of TOC, I/(Ca+Mg), and Fe_{HR}/Fe_T ratios.

The third phase encompasses depths of 60 to 79 m, encapsulating the late and concluding phase of the SPICE event: (IV) Between 60-65 m, corresponding to the SPICE event's late stage, a minor peak in carbon isotopes is observed, accompanied by slight increases in TOC and I/Ca ratios, a slight decrease in the Fe_{HR}/Fe_T values, and further enrichment of major and trace elements took place. (V) From 65 to 79 m, this stage occurs after the

conclusion of the SPICE event. The carbon isotope curve returns to the baseline, while enrichment of major and trace elements persists, and TOC maintains relative stability. I/(Ca+Mg) and Fe_{HR}/Fe_T ratios also continue the overall trend of the baseline.

5.2 Assessing terrigenous influence

The Eilean Dubh Formation exhibits pronounced terrigenous material input. Therefore, it is necessary to perform terrigenous influence stripping on elements in the samples that are susceptible to detrital influence, essentially examining whether the content of these elements is predominantly governed by detrital flux.

A straightforward approach to assessing whether the content of a certain element is predominantly controlled by detrital flux involves comparing trace elements with aluminum or titanium (Calvert and Pedersen, 1993, Tribovillard et al., 1994, Hild and Brumsack, 1998, Böning et al., 2004). If a strong correlation is observed, and the concentration of the trace element is not significantly deviant from the average shale concentration, it can be inferred that the trace element primarily originates from terrigenous sources and cannot be utilized for palaeoredox analysis. Generally, trace element concentrations are conventionally normalized to aluminum content (Calvert & Pedersen, 1993) since aluminum is considered an indicator of the terrigenous aluminosilicate fraction in sediments and is thought to be immobile during diagenesis. However, the aluminum content during Stage I of the Eilean Dubh Formation is notably low, with half of the values falling below the detection limit, and the remaining values hovering around the detection limit, which could potentially exaggerate the results of element normalization. Therefore, this study employs titanium as an alternative element to aluminum for element normalization, as it is another characteristic indicator of terrigenous material sources, and some studies have suggested that titanium has more resistance to authigene compared to aluminum (Wei et al., 2003). The titanium content in the Eilean Dubh Formation is well above the detection limit and demonstrates a strong correlation

with aluminum concentrations (r = 0.87), validating its behavior as an indicator of terrigenous components.

To delve further, when trace elements exhibit the potential for mixed sources, where detrital and authigenic influences simultaneously affect trace element concentrations, the authigenic fraction can be estimated as the excess portion above the detrital background concentration. The detrital component of element X in the sample can be approximated as follows: $X_{detrital} = (X_{bg} / Ti_{bg}) \times Ti_{sample}$ (where X_{bg} represents the background value of element X, and X_{sample} is the measured value of element X in the sample). Clearly, the authigenic fraction of element X is naturally: $X_{auth} = X_{sample} - X_{detrital}$ (Tribovillard et al., 2006; Scholz et al., 2018). Hence, the background value of element X is a critical factor in this step. Generally, "average shales" (Turekian and Wedepohl, 1961), Post-Archean Australian shale (PAAS) (Taylor and McLennan, 1985), or upper continental crust (UCC) (McLennan, 2001) are used as detrital background values. However, this approach has faced much criticism (Reimann and De Caritat, 2005; van der Weijden, 2002; Brumsack, 2006; Cole et al., 2017), primarily because these global background values may not necessarily represent the local/regional sediments of the study area. Secondly, average crustal rocks or shales may also contain diagenetic components, potentially introducing systematic errors in the estimation of trace elements. This is especially relevant in the Eilean Dubh Formation, where the rapid increase in Al, Ti and Th from stages I to II indicates a dramatic change in detrital input. Therefore, selecting a background value from a local source can reduce errors in estimation (Paul et al., 2023). In this study, a local terrigenous influence baseline is utilized, with enrichment beyond this baseline indicating elements influenced by redox controls. The calculation method is as follows: $X_{local} = (X / Ti)_{minimum}$ (Fig. 16). Correspondingly, the calculation of X_{auth} is changed to $X_{auth} = X_{sample} - (X_{local} * Ti_{sample})$.

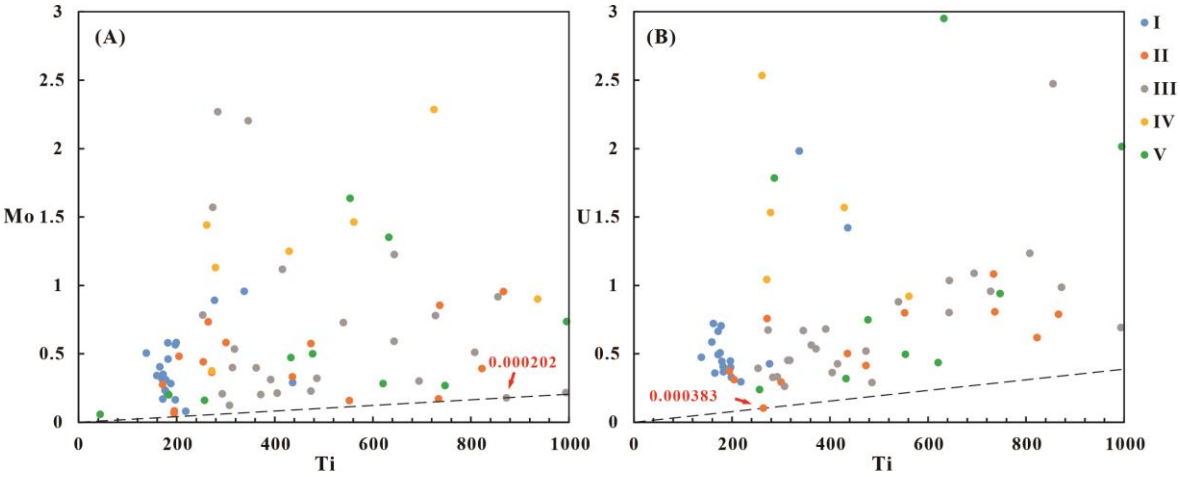

Fig. 16 The local background baselines (dashed line) of detrital molybdenum (A) and uranium (B)

Furthermore, reconstructing palaeoredox conditions through trace element concentrations requires evaluating whether they are relatively enriched or depleted. To succinctly convey the normalization process and outcomes, the Enrichment Factor (EF) is employed to denote the normalized elements, calculated as element $X_{EF} = (X_{auth}/Ti_{sample}) / X_{local}$. An X_{EF} greater than 1 indicates relative enrichment of element X compared to average shales, while an X_{EF} less than 1 signifies depletion of element X (Tribovillard et al., 2006).

5.3 Redox analysis

5.3.1 Molybdenum–uranium covariation

Due to the characteristics of molybdenum (Mo) and uranium (U), they prove to be particularly valuable in the analysis of palaeoenvironment. Both elements exhibit conservative behavior under oxic conditions and have long residence times in seawater (U at about 450 kyr and Mo at about 780 kyr). Thus, the concentrations of these two elements in global seawater remain nearly uniform (Algeo and Tribovillard, 2009). Furthermore, their concentrations in planktonic organisms are generally low, making any enrichment in sediment or sedimentary rock typically attributable to their authigene from seawater. For both elements, the enrichment is greatly facilitated by anoxic conditions (Algeo and Tribovillard, 2009). Despite these similarities, there are significant differences in the

behaviors of molybdenum and uranium under reducing conditions, which can result in variations in their abundance in marine sediments: the enrichment of U_{auth} commences at the Fe^{2+} - Fe^{3+} redox boundary, preceding the requirement for the presence of H_2S necessary for Mo_{auth} enrichment (Helz et al., 1996; Zheng et al., 2002); the transfer of Mo_{auth} into sediments can be increased by the shuttle of particulate manganese-Ferrum-oxyhydroxide (Murray, 1975; Crusius et al., 1996), In contrast, U_{auth} remains unaffected by this mechanism.

Given these, the analysis of Mo_{auth} - U_{auth} covariation patterns can be valuable indicators of palaeoenvironments and processes within palaeoceanographic systems. Mo_{auth}-U_{auth} covariation can obtain information regarding variations in benthic redox conditions and the operation of particle shuttle within the water column (Algeo and Tribovillard, 2009) (Fig. 17A).

Through Enrichment Factors (EFs), we can compare the enrichment degree of Mo_{auth} and U_{auth} in the samples. Within an open marine environment, the transition from suboxic to anoxic benthic redox conditions promotes the enrichments of both Mo_{auth} and U_{auth}. However, the relatively higher accumulation of Mo EF results in a gradual increase of Mo EF / U EF value, transitioning from 0.1–0.3 times the seawater molar ratio to 1.0–3.0 times that value. This indicates that when redox conditions at the sediment/water interface hover near suboxic conditions, U EF predominates over Mo EF. Conversely, in environments with strongly reducing and/or frequently sulfidic benthic conditions, Mo EF takes precedence over U EF (Algeo and Tribovillard, 2009).

In Mo_{auth}-U_{auth} enrichment patterns within euxinic conditions, the mode of enrichment is contingent on the effectiveness of the particle shuttle. In smaller basins with deeper or highly variable chemoclines, the operation of particle shuttle may enhance the transfer of soluble molybdenum to the sediment/water interface, resulting in higher and uniform

Mo_{auth}/U_{auth} value. In basins characterized by shallow and stable chemoclines, the particle shuttle is less likely to effectively transport molybdenum. Additionally, when the molar ratio of Mo/U closely approximates that of seawater, the Mo_{auth}/U_{auth} ratio in sediments is relatively high. However, as molybdenum in the restricted water columns becomes progressively depleted through sedimentary processes without significant replenishment, the Mo_{auth}/U_{auth} ratio in sediments proportionally decreases (Algeo and Tribovillard, 2009; Tribovillard et al., 2012). Therefore, the molybdenum–uranium covariation can serve as an indicator of the water depths and degree of openness in sedimentary environments (Fig 17A).

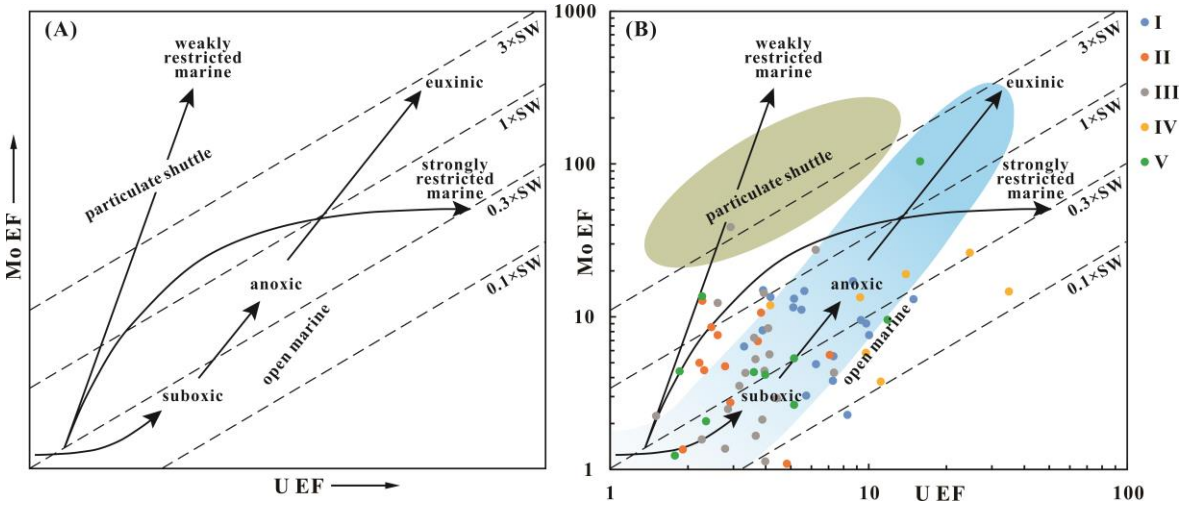

Fig. 17 (A) The model of enrichment patterns and covariation of (Mo_{auth} /U_{auth}) ratios. The diagonal dashed lines represent the (Mo/U) molar ratio of seawater (SW) (modified after Algeo and Tribovillard, 2009); (B) The Mo-U covariation model for sample data input, the particulate shuttle zone and the open marine zone were modified according to Tribovillard et al., (2009).

The Mo EF and U EF data of samples were input into the Mo-U covariation model proposed by Algeo and Tribovillard (2009) (Fig. 17B). Most samples fall within the suboxic to anoxic range, except for sample 76 from Stage V, which is in the euxinic threshold. Stage I and IV indicate sedimentary environments with partial restriction, while stage II, III, and V represent relatively open marine. Additionally, some samples from stage II, III, and V were near the particulate shuttle zone, indicating deeper-water environments.

5.3.2 Assessing the utility of Fe speciation

The I/(Ca+Mg) ratios of the samples fell within the range of 0.15 to 0.4, aligning with the suboxic threshold as delineated by Uahengo et al. (2020), with dissolved oxygen concentrations ranging from ≥ 3 μM to ≤ 10 μM. However, converting this to the widely accepted redox condition standard proposed by Tyson and Pearson (1991) situated these samples within the suboxic to anoxic threshold (Section 1.3), corresponding to values ≥ 0.072 ml O_2 / l H_2O to ≤ 0.24 ml O_2 / l H_2O (under conditions of 20 ℃ and 101.3 kPa). The calculation process is as follows:

X_1 ml O_2 / l H_2O = (X_2 μM * 8.31 J / (mol·K) * T) / P / 1000

(X_1 and X_2 are the concentrations of oxygen in different units, T represents temperature, P stands for pressure, and this study chose normal temperature and standard pressure: T = 293.15 K, P = 101.325 kPa, and 8.31 J/(mol·K) is the ideal gas constant from Henry's law) (Sander, 2015).

Currently, Fe speciation techniques find widespread application in the redox analysis of siliciclastic-rich samples such as shales and mudstones (LeRoy et al., 2021, 2022; Gill et al., 2011; 2021). However, their utilization in carbonate formations remains limited, primarily due to the absence of insufficient siliciclastic components (Clarkson et al., 2014). Fe speciation holds substantial potential for indicating redox changes within carbonate rocks, and there have been a few implementations in carbonate-rich marine sediments (März et al., 2008, Kendall et al., 2010, Zerkle et al., 2012). While Clarkson et al. (2014) calibrated the guiding behavior of Fe speciation in carbonate-rich samples, its practical application requires further enhancement. Therefore, this study aims to validate the practicality of Fe speciation within the carbonate system using the I/(Ca+Mg) ratio, a stable carbonate redox proxy. This validation is conducted on high-purity carbonate rock samples (exceeding 90%), thus contributing to enhancing a potential archive for the reconstruction of palaeoenvironments in carbonate systems.

The Fe_{HR}/Fe_T ratio lacks the ability to finely discriminate redox conditions. Within the conventional interpretive framework of Fe speciation, the terms “oxic” and “anoxic” simply denote the presence or absence of oxygen in the water column, rather than specifying its absolute concentration. In modern sediments, the oxic threshold of Fe_{HR}/Fe_T encompasses both traditional oxic and dysoxic intervals. A ratio exceeding 0.38 incorporates all oxygen-depletion states, including suboxic, anoxic and euxinic conditions (Raiswell et al., 2018; LeRoy et al., 2021). In all the samples, the Fe_{HR}/Fe_T ratios concur with the redox indicative behavior of the I/(Ca+Mg) values (also Mo EF-U EF covariation), affirming the reliability of its capacity to indicate redox changes when Fe concentrations exceed 0.5 wt% in carbonate system. Additionally, the ratios of Fe_{HR}/Fe_T exhibited a strong correlation with the I/(Ca+Mg) ratios (Fig. 15; Fig. 18). Perhaps Fe speciation holds the potential to differentiate oxygen-depletion conditions. However, it's worth noting that these thresholds are likely to vary between siliciclastic and carbonate systems. In carbonate rocks, a value below 0.38 signifies an oxic environment, whereas in siliciclastic sediments, the threshold is within 0.22 and the range of 0.22-0.38 is considered an equivocal redox condition (Rachel et al., 2015). Furthermore, Fe_{py}/Fe_{HR} ratios are significantly below 0.7, signifying extensive ferruginous environments for Durness SPIECE event, rather than euxinic condition.

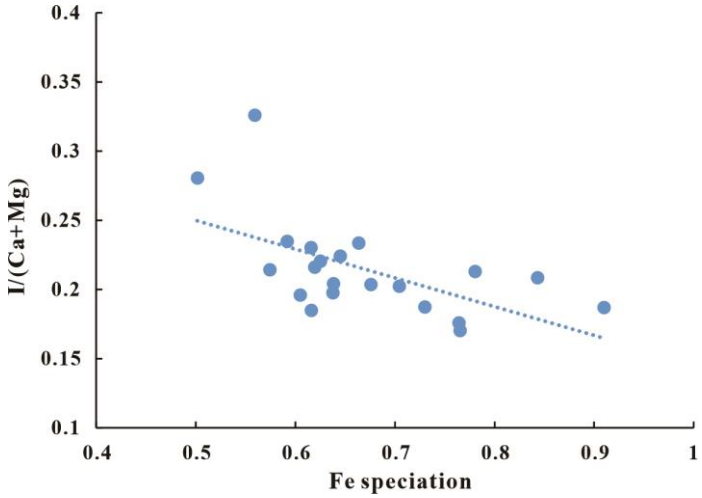

Fig. 18 The cross plot of Fe_{HR}/Fe_T values with I/(Ca+Mg) ratios

5.3.2 The redox fluctuation of the Durness SPICE event

Among the three redox proxies, the I/(Ca+Mg) ratio, Fe speciation, and molybdenum-uranium covariation, only the I/(Ca+Mg) ratio provides an indication of absolute concentrations in the sedimentary environment. It exhibits two intervals of relative oxygenation during Stages II and IV (Fig. 15), which correspond to two peaks in TOC. Furthermore, the variations in I/(Ca+Mg) ratios relative to TOC content show consistent trends across all five stages of the Durness SPICE event (Fig. 19A), indicating a correlation between I/(Ca+Mg) ratios and TOC (r=0.6). The process of iodine entering the carbonate lattice is unrelated to TOC (Section 1.4.1), suggesting that the increase in TOC is associated with elevated oxygen levels in the sedimentary environment, independent of iodine's chemical dynamics. Moreover, the overall decreasing trend in I/(Ca+Mg) ratios (Fig. 15) suggests a gradual depletion of oxygen in the sedimentary environment during the Durness SPICE event.

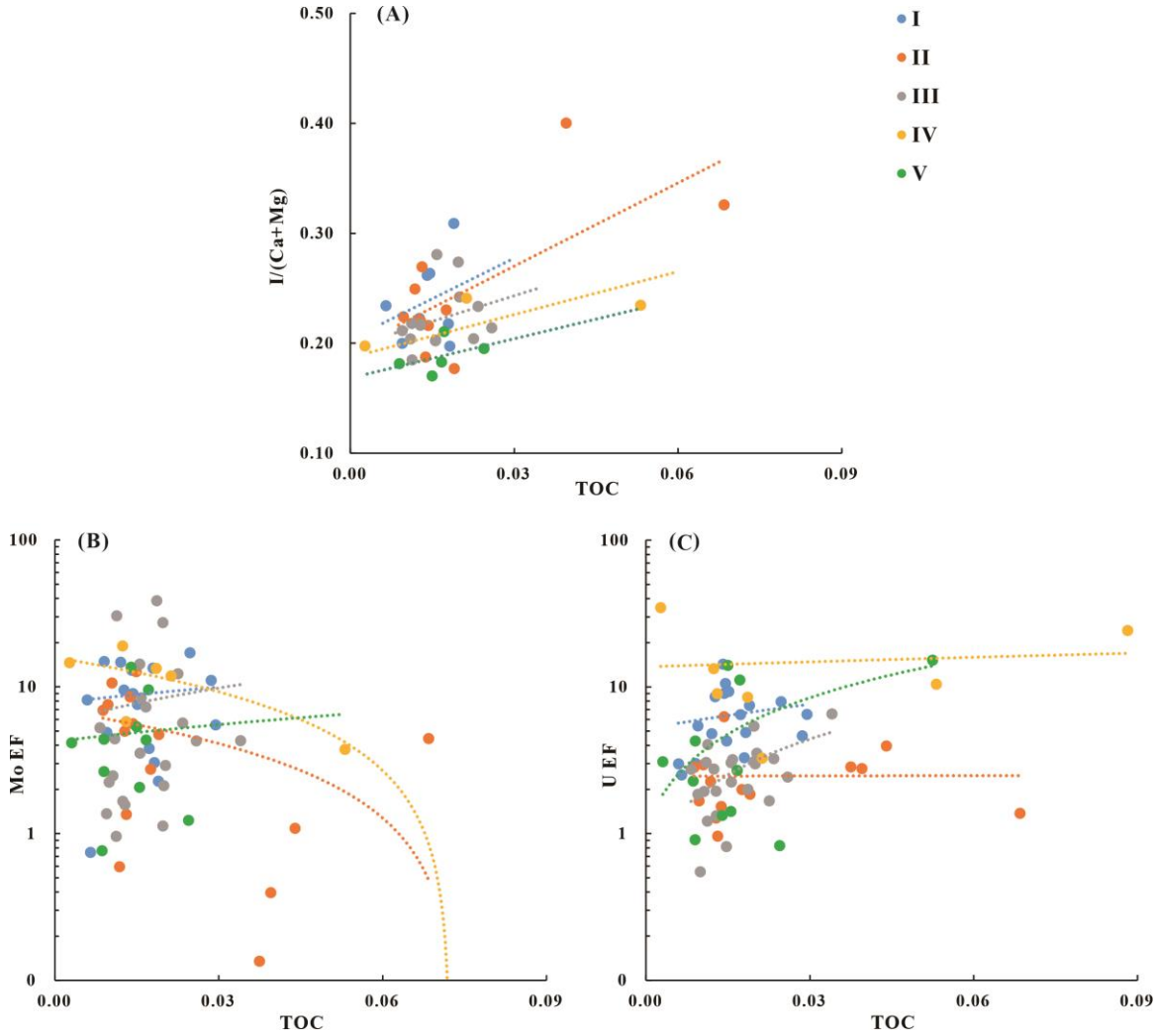

Fig. 19 The cross plots of redox proxies with TOC: (A) I/(Ca+Mg) vs. TOC; (B) Mo EF vs. TOC; (C) U EF vs. TOC.

In contrast to iodine, the enrichment of molybdenum and uranium is highly correlated with TOC content, as organic matter serves as a vector for aqueous Mo and U removal to sediments in anoxic environments (Section 1.4.3, Tribovillard et al., 2004; Algeo and Tribovillard, 2009). Mo EF and U EF exhibit distinct trends during Stages II and IV (Fig. 19B, C), where the enrichment of Mo and U weakens with increasing TOC content compared to background values in other stages, providing evidence for decreasing anoxia. Additionally, the Mo EF vs. TOC plot excluded sample 76 due to its exceptionally high value (103, compared to an average of 7.7 for other samples). Typically, significant Mo enrichment relative to background values indicates the onset of euxinic conditions (Tribovillard et al., 2006), suggesting that sample 76 likely represents localized euxinia,

consistent with its behavior in the molybdenum-uranium covariation model. However, excluding sample 76, Mo EF does not exhibit significant increases from Stage I to V (Fig. 15), suggesting that widespread euxinia had not occurred. Uranium's redox behavior is different, as it begins to enrich in anoxic conditions (Tribovillard et al., 2006). From Stage IV onwards, a noticeable enrichment in uranium can be observed (Fig. 15), with U EF increasing from an average of 3.8 in the preceding three stages to 8.9, indicating the transition of the Durness SPICE event from suboxic to anoxic conditions.

Collectively, the integrated redox proxies of the I/(Ca+Mg) ratio, Fe speciation, and molybdenum-uranium covariation reveal consistent redox fluctuations during the Durness SPICE event. The overall trend of the event involves a gradual depletion of oxygen, transitioning from initial suboxic condition to an anoxic environment by Stage IV, with potential euxinia occurring in localized water columns. Furthermore, brief intervals of relative oxygenation during Stages II and IV strongly correlate with increased TOC.

5.4 Analysis of the Durness SPICE event processes

5.4.1 Stage I

There is substantial evidence of evaporites in Stage I, characterized by crystal-shaped vugs frequently filled with calcite, which is inferred as replacements for gypsum. Raine and Smith (2017) classified this stage as a shallow-water Sabkha facies developed on a tidal flat, marking LST (Fig. 14), with aeolian cycle caps initiating as early as Stage I. Remarkably, this Stage I lacks any discernible terrestrial clastic imprints, as signified by exceedingly diminished concentrations of aluminum (mean: 0.16 wt%) and titanium (mean: 205 ppm), with carbonate concentrations exceeding 90% (Pruss et al., 2019). The molybdenum-uranium covariation suggested a partially restricted environment, consistent with the sedimentary background. Tidal flats are often associated with lagoons and barrier islands, thereby forming a semi-restricted tidal flat-lagoon system. The I/(Ca+Mg) ratios

signify suboxic conditions during stage I. Nonetheless, it is essential to note that diagenetic processes may potentially lower iodine concentrations in sediments (Section 1.4.1). Furthermore, due to the low Fe content, data concerning Fe speciation are absent for this stage. In general, Fe in sediments is derived from diagenesis under anoxic conditions or hydrothermal vents (Poulton and Canfield, 2011) (there is no evidence of hydrothermal activity within the study area, Pruss et al., 2019), and both TOC and FeT content below 0.5 wt% indicate a potentially oxic environment (Section 1.4.2). Consequently, the potential higher I/(Ca+Mg) ratios and low Fe concentrations during stage I imply a suboxic or potentially oxic-suboxic sedimentary environment. Therefore, Stage I represented shallow and semi-restricted Sabkha facies without continental input, developing on a tidal flat (Fig. 20). At this juncture, the SPICE event had not yet commenced, and the marine environment was characterized as suboxic or potentially oxic-suboxic. Stage I provides essential local information about the sedimentary environment, forming the foundational basis for subsequent SPICE event elucidations.

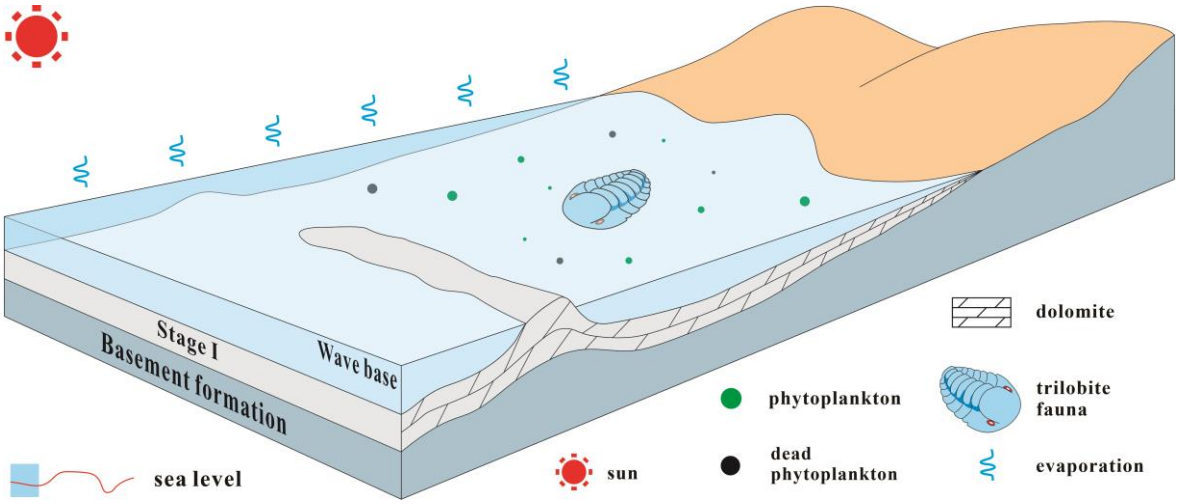

Fig. 20 The conceptional model of stage I (LST)

5.4.2 Stage II

In Stage II, evaporites were not observed, and the predominant lithology consisted of laminated limestone. There were localized occurrences of stratiform intraclast breccias and

a little terrestrial quartz, with occasional presence of stromatolites. Raine (2010) identified this stage as a TST, indicating a relative sea-level rise. The deepening sedimentary environment was also confirmed by molybdenum-uranium covariation. The shift towards an open marine setting may be attributed to the sea level having surpassed barrier islands, transforming the semi-restricted tidal flat environment into open marine. Stage II marks the onset of the SPICE event, characterized by significant environmental fluctuations, including abrupt increases in aluminum (mean: 0.67 wt%) and titanium (mean: 432 ppm) concentrations and a brief spike in TOC and I/(Ca+Mg) ratios.

The sudden increase of Al and Ti is undoubtedly attributed to the influx of terrigenous detritus, whereas the TOC reflects changes in marine primary productivity. The majority of organic carbon in sediments comes from the sinking particles of surface organic matter, with a minor contribution from continental organic carbon in marginal marine settings (Schoepfer et al., 2015). The lack of a strong correlation between TOC and Ti (r=0.17) indicates that TOC content is primarily controlled by marine productivity rather than terrestrial organic materials. The increase in primary productivity results from the extensive proliferation of plankton. Initially, the augmented photosynthetic activity of phytoplankton engendered a transient spike in oceanic oxygenation, and this was discerned through the brief elevation of the I/(Ca+Mg) ratios. However, the subsequent microbial degradation of dead planktonic biomass consumed a significant amount of oxygen, resulting in widespread or localized anoxia. The occurrence of anoxic events associated with increased primary productivity is widely documented (Jenkyns, 2010). Furthermore, the I/(Ca+Mg) ratios returned to Stage I baseline after experiencing oxygenation fluctuations, and there is no significant increase in Mo EF and U EF, indicating that Stage II still operated under suboxic conditions. However, following the return of TOC to baseline, the I/(Ca+Mg) ratios decreased, indicating an expansion of anoxic conditions. It is noteworthy that the peak of the SPICE event roughly corresponded to the Maximum Flooding Surfaces (MFS) during this stage.

The increase in productivity is likely attributed to rising sea levels, resulting in the upwelling of nutrient-rich deep-sea waters, thus promoting eutrophication of the water column. The Cambrian is a relatively warm period, marked by the sluggish circulation of global ocean currents, conducive to ocean stratification and the formation of nutrient-rich deep waters (Wilde and Berry 1984; Weissert 1989). Early Paleozoic anoxic events led to the burial of substantial organic matter in the deep sea (Wilde and Berry 1984; Saltzman et al., 2004), and Cowan et al. (2003) proposed that sea-level rise could trigger substantial nutrient pulses in the ocean. Cases of anoxic events resulting from the upwelling of nutrient-rich deep-sea water have been well-documented (Arthur et al., 1987; Vincent and Berger, 1985; Woods et al., 2011). Another common source of nutrients in the ocean is detrital input from continental weathering (Kump and Arthur 1999; Saltzman et al., 2004). However, its likelihood is diminished in this stage, as there is only sporadic evidence of terrigenous detritus within the stratum, with irregular dispersion.

In summary, Stage II represents the onset of the Durness SPICE event and is marked by a rising sea level that triggered an increase in marine primary productivity (Fig. 21). After a brief oxygenation, the extensive mortality of plankton, coupled with microbial decomposition, consumed oxygen, resulting in suboxic conditions. The carbon reservoirs of nature are in equilibrium, with biological processes preferentially absorbing ^{12}C, resulting in the enrichment of ^{13}C in seawater (as discussed in Section 1.1). During the dominance of photosynthesis, microbial decomposition could effectively return ^{12}C to the seawater, which was also the reason why carbon isotopes could maintain the baseline during the early stages of SPICE. However, as oxygen gradually diminished, microbial decomposition rates slowed down, leading to a gradual reduction in the release of ^{12}C. This caused an increase in the carbon isotope of carbonate rocks. The difference between ^{12}C absorbed and released by phytoplankton reached its peak at the MFS, which corresponds to the zenith of deep-sea nutrient supply. This indicates that, even though the seawater was in

a suboxic state, abundant nutrients continued to support the modest proliferation of phytoplankton, which exceeded the rate of microbial decomposition.

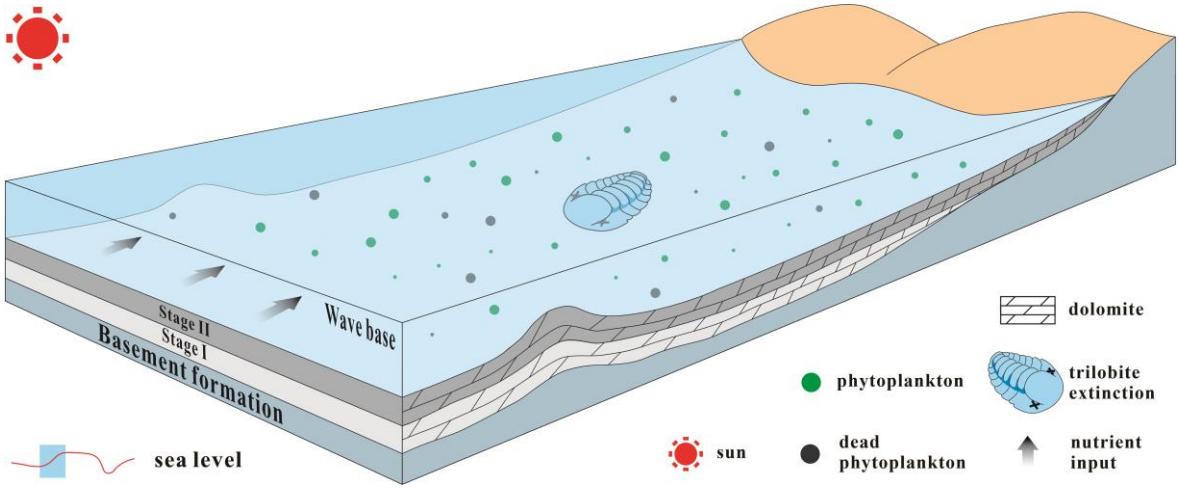

Fig. 21 The conceptional model of stage II (TST)

5.4.3 Stage III

In Stage III, the lithology of the lower part inherited from Stage II, primarily consists of laminated dolomites. From the latter half onward, river channels, karst, microbialites and evaporites development began, with more recording of quartz sands. Raine and Smith (2012) designated the lower laminated dolomites as the HST, followed by the falling-stage systems tract (FSST) after RSME (Fig. 14), marking the top of the HST and representing a relative sea-level decrease (Plint and Nummedal, 2000). The geochemical characteristics of Stage III inherited from Stage II indicated that the sedimentary environment did not undergo significant changes. Aluminum (mean: 0.75 wt%) and titanium (mean: 503 ppm) concentrations increased slightly, in line with increased detrital input. The covariation of molybdenum and uranium maintains the characteristics of open deep-water sedimentation, with no significant increase in Mo EF and U EF, indicating that Stage III continued to exhibit suboxic conditions, but with a slowly increasing I/(Ca+Mg) ratios, suggesting intensifying suboxic condition trending towards anoxia.

TOC of stage III, averaging 0.013 wt%, hovered near the baseline, and was lower than the values observed during Stage II (mean: 0.022 wt%), This suggests that marine productivity declined following the drop in sea level, leading to a further reduction in the proliferation rate of phytoplankton. Consequently, the absorption of ^{12}C gradually weakened relative to its release, resulting in a corresponding decrease in carbon isotope values, eventually returning to baseline. However, the decomposition of phytoplankton accumulated in Stage II continued, leading to a persistent increase and expansion of marine anoxia.

Stage III represents the period following the peak of the Durness SPICE event, characterized by a slow decrease in sea level (Fig. 22). Marine primary productivity decreased, and carbon isotope values gradually returned to baseline. Concurrently, phytoplankton continued to perish, exacerbating suboxic conditions in seawater.

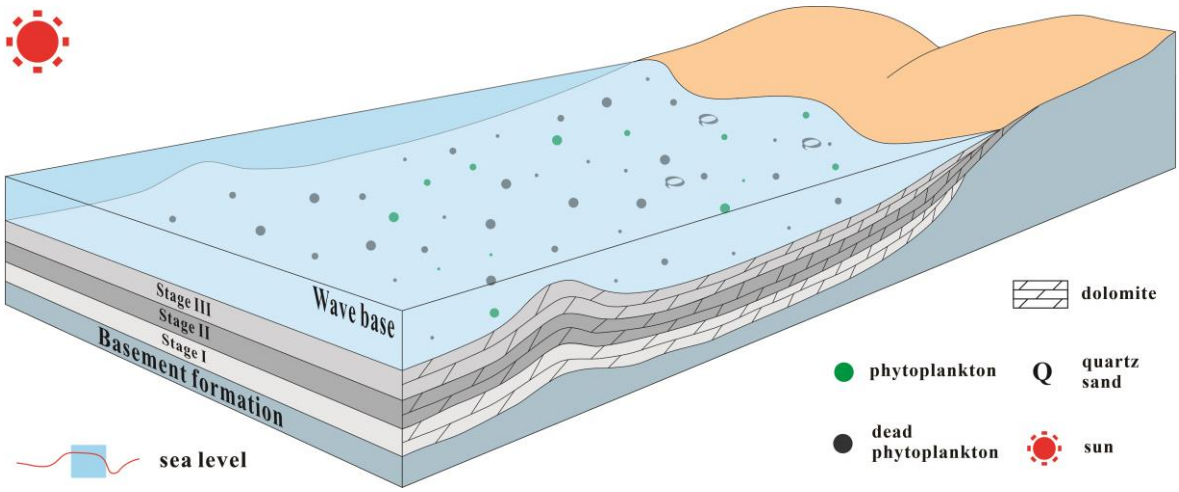

Fig. 22 The conceptional model of stage III (HST and FSST)

5.4.4 Stage IV

Stage IV represents a significant portion of the Eilean Dubh formation: the Sauk II–III Supersequence Boundary. This is characterized by a thin, meter-scale shallow-upward peritidal cyclic interval composed of stromatolites, intraclast dolomites, teepee structures, karst at the surface, and abundant quartz sands and evaporites.

In stage IV, the presence of significant evaporites, primarily gypsum and/or anhydrite, along with localized evaporite pseudomorphs, provided evidence of a shallower sea level compared to stage I (Fig. 14). This observation is further substantiated by the Mo-U covariation trends in stage IV data, which exhibit a stronger affinity toward restricted marine conditions. TOC experienced a transient elevation, accompanied by slight increases in the I/(Ca+Mg) ratios. These characteristics resemble the features of stage II, both indicating brief oceanic oxidation followed by a return to baseline values. Likewise, during stage IV, TOC exhibited very low correlations with aluminum (r=0.03) and titanium (r=0.04), implying that the increase in TOC is not a result of terrigenous organic input but rather signifies a temporary enhancement in marine primary productivity.

In the broader context of global research on the SPICE event, some studies have attempted to explore its relationship with changes in sea level during the Sauk II-III Supersequence Boundary (Glumac and Walker, 1998; Saltzman et al., 1998, 2000, 2004). These investigations proposed a connection between the appearance of the SPICE event and increased surface runoff and/or enhanced continental weathering resulting from the lowering of sea levels. In other words, alterations in weathering patterns due to the eustatic decline were believed to have introduced nutrient-rich terrestrial material into seawater, leading to increased marine primary productivity and carbon isotope. This explanation is reasonable because a distinguishing characteristic of the Sauk II-III Supersequence Boundary is the influx of abundant siliciclastic detritus, attesting to intensified input of terrestrial material. Concentrations of aluminum (mean: 0.95 wt%) and titanium (mean: 533 ppm) in samples from stage IV are indeed higher compared to stage III, and the lithological records also documented a significant influx of quartz sand, thereby lending further support to this perspective.

Furthermore, it's noteworthy that during stage IV, there was no conspicuous increase in Mo

EF, while U EF significantly increased. This signifies that U began to enrich during this stage compared to background values, marking the onset of anoxia in the water column (Tribovillard et al., 2006). This suggests that, due to the elevated ocean productivity experienced once again, the study area's seawater transitioned from suboxic to anoxic conditions. However, the enrichment of Mo suggests an euxinic environment (Tribovillard et al., 2006), signifying that stage IV had not yet reached euxinic levels.

stage IV marks the conclusion of the Durness SPICE event, corresponding to a regression period (Fig. 23), characterized by a more restricted environment compared to stage I. Enhanced continental weathering input brought a significant influx of terrestrial detrital, triggering intensified marine productivity, exacerbating oxygen depletion, and transitioning the environment from suboxic to anoxic conditions. Stage IV had a relatively short duration and heightened primary productivity led to a subtle carbon isotope peak.

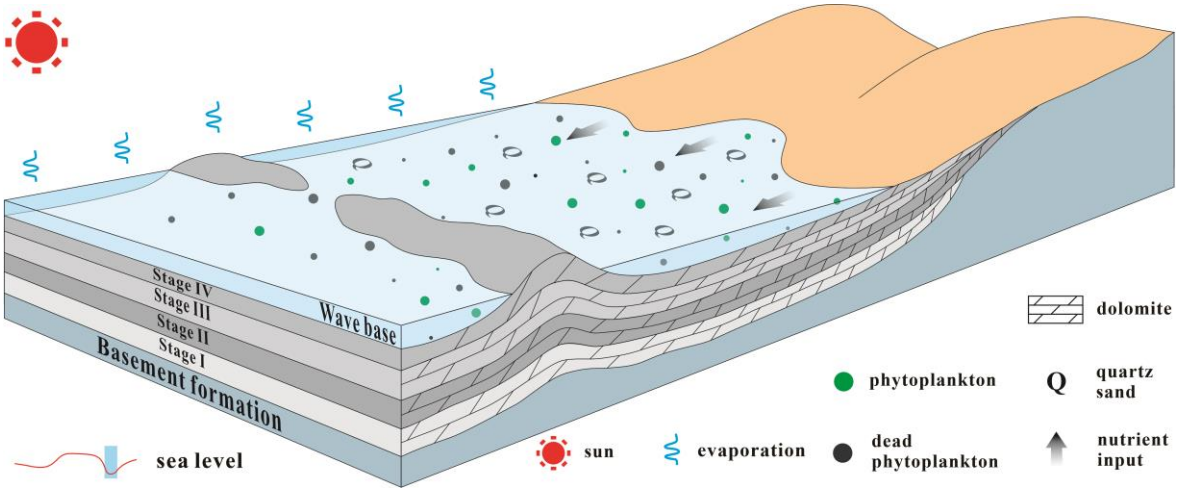

Fig. 23 The conceptional model of stage IV (the Sauk II-III Supersequence Boundary)

5.4.5 Stage V

Stage V represents the post-SPICE phase, characterized by a reduction in evaporites and quartz sands, with visible stromatolites and carbonate detritus. Ranie and Smith (2017) classified this stage as a Transgressive Systems Tract (TST), in which the sea level

gradually rose in comparison to Stage IV (Fig. 24), transitioning into an open environment, in line with the Mo-U covariation data. During this stage, TOC remained at baseline, and aluminum and titanium concentrations retained values inherited from Stage IV. The I/(Ca+Mg) ratios gradually decreased. These features indicated environmental stability, with the continued decomposition of phytoplankton further exacerbating marine anoxia.

U EF ceased to increase, and Mo EF continued to maintain the baseline values observed in stage I, suggesting that the marine anoxia had not yet progressed to euxinic conditions, in line with the data from Fe_{py}/Fe_{HR}. However, it is worth noting that sample 76 (at 77.3m depth, the end of the research stratum) exhibits exceptionally high Mo EF values and lies within the euxinic threshold in the molybdenum-uranium covariation model, indicating the potential presence of localized euxinic conditions. After SPICE, oceanic anoxia continued to spread and intensify, with the possibility of developing into widespread euxinic environments.

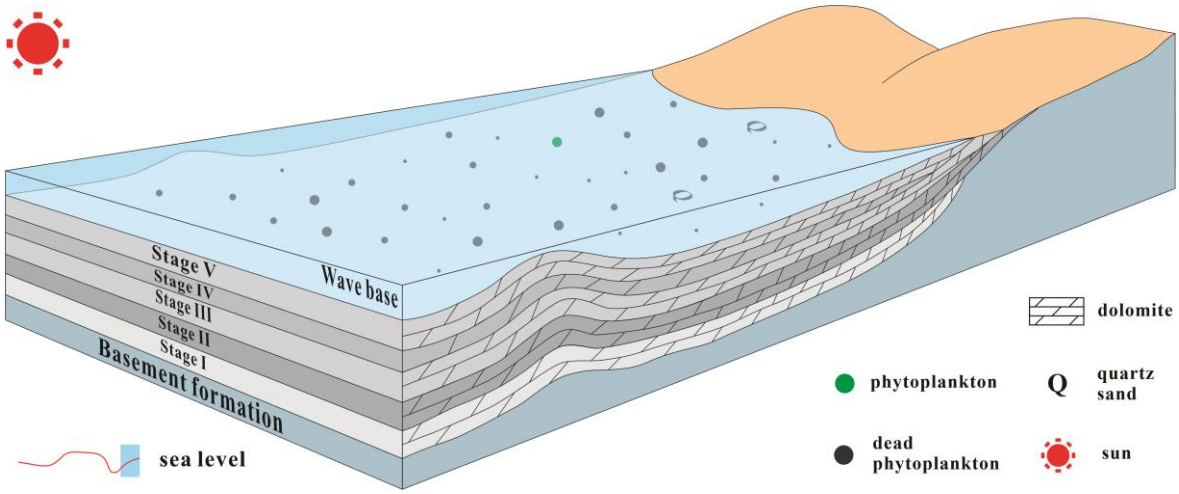

Fig. 24 The conceptional model of stage V (TST)

5.5 The positions of the SPICE events

According to Ranie and Smith (2017), the carbon isotope peak of the Durness SPICE event was proposed to occur at the Sauk II-III Supersequence Boundary. However, the carbon

isotope curve in this study suggested that the peak of the SPICE event occurred below the Sauk II-III Supersequence Boundary, near the MFS. Meanwhile, the Sauk II-III Supersequence Boundary in Durness exhibited a subtle carbon isotope peak, consistent with the observations documented by Pruss et al. (2019) (Fig. 11).

In many of the SPICE cases associated with the Sauk II-III Supersequence Boundary, this boundary was predominantly positioned towards the later stages of the SPICE event. The peak of the SPICE event partly occurred within the Sauk II-III Supersequence Boundary and partly before it (Saltzman et al., 2004; Woods et al., 2011). This distinction is largely influenced by regional latitude. At the southernmost tip of the Laurentia (approximately at 30° S), on the English Midland Platform adjacent to Scotland, the Outwoods Shale Formation recorded an Avalonia SPICE event highly analogous to the Durness SPICE event. Notably, both events exhibit a subtle second peak, referred to as excursion 2 by Woods et al. (2011), corresponding to sea-level decline and quartzite input, which aligns with the recognized characteristics of the Sauk II-III Supersequence Boundary. Conversely, in the central Laurentia, near the equator, SPICE events in Iowa and Minnesota peaked within the Sauk II-III Supersequence Boundary (Saltman et al., 2004). In the northern portion of the Laurentia, around 15° N in Utah, the peak of the SPICE event within the Sauk II-III Supersequence Boundary was less pronounced (Saltman et al., 2004).

Based on current understanding, the initiation of the SPICE event appeared to be driven by increased marine primary productivity induced by nutrient supply, leading to enhanced ^{12}C biological uptake. Both classic sources of marine nutrients were evident in the Durness SPICE event, namely deep nutrient-rich upwelling and intensified continental weathering. In warmer equatorial regions, continental weathering holds a dominant advantage compared to colder areas because lower temperatures influence the presence of precipitation, vegetation growth, decomposition rates, and the thickness of permafrost layers. These factors hinder chemical weathering and substances transport (Xiong et al.,

2022). Consequently, equatorial regions are more likely to experience higher levels of weathering following regressions, bolstering its control over SPICE event, with peaks occurring during the sea-level regression phases of the Sauk II-III Supersequence Boundary. Conversely, in high-latitude regions, the elevation in productivity resulting from rising sea levels tends to take precedence, leading to SPICE event peaks occurring during transgressions prior to the Sauk II-III Supersequence Boundary. Moreover, Pulsipher et al. (2021) recently compiled global SPICE event data and pointed out that the regional expression of SPICE events is closely tied to latitude. Specifically, $\delta^{13}C$ peaks recorded in sections at palaeolatitudes (approximately 500 Ma) of 30 to 60°S (no records at 30 to 60°N) are basically 1 to 2‰ lower compared to tropical SPICE events. The Durness SPICE event conforms to this pattern. This likely stems from the limited influence of latitude on sea-level rise, which resulted in a stable magnitude of carbon isotope elevation. In contrast, the enhanced weathering caused by the Sauk II–III regression had a more significant elevation in carbon isotope values but was also strongly affected by latitude. In tropical regions, continental weathering primarily governed SPICE events, leading to larger carbon isotope peaks surpassing those associated with sea-level rise, whereas in colder regions, the impact of continental weathering was less pronounced, and the peaks were primarily controlled by sea-level rise, resulting in lower peak values. This further underscores that despite the global scale of SPICE events, their regional expression is latitude-dependent.

This study has integrated the occurrences of several SPICE events, substantially corroborating this perspective. However, most of the SPICE event records did not mark the Sauk II–III Supersequence Boundary. Consequently, such data estimated the position of the carbon isotope peak based on the assumption that the Sauk II–III Supersequence Boundary occurred near the end of the SPICE events, denoted by circular markers in Figure 25, serving as auxiliary evidence. Cases with well-defined positioning of the Sauk II–III Supersequence Boundary were denoted by stars. Nonetheless, this theory is currently in the hypothesis development stage, and additional global evidence from SPICE events

associated with the Sauk II-III Supersequence Boundary is required to substantiate the validity of this viewpoint.

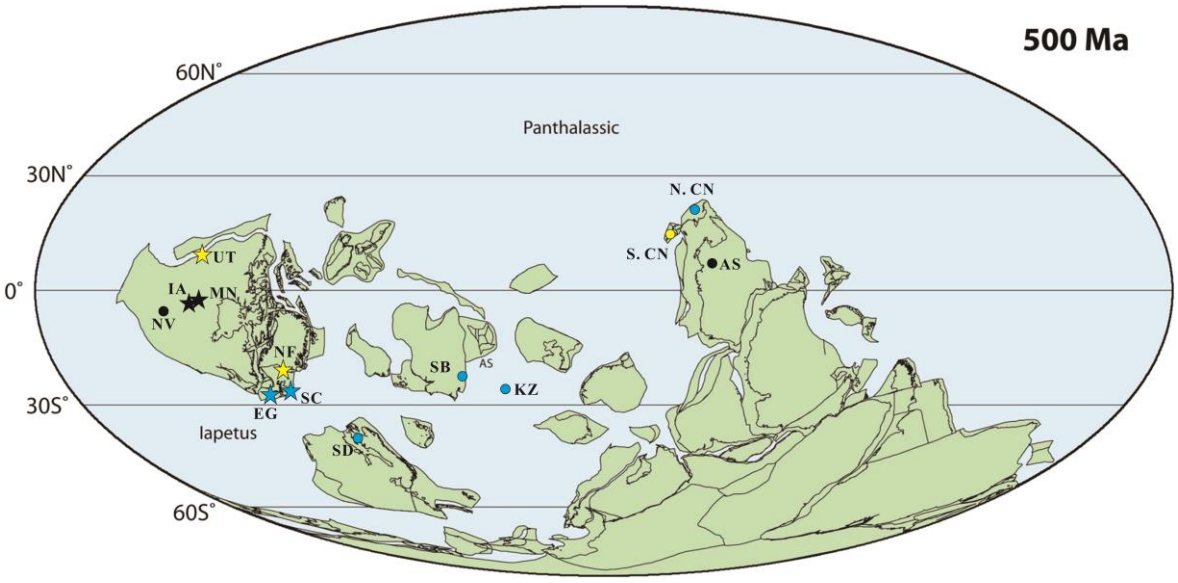

Fig. 25 The global integration of SPICE event locations. In the Sauk II–III Supersequence Boundary, SPICE events with subtle carbon isotope peaks were represented in blue, those with less distinct peaks in yellow, and prominently expressed peaks in black (SC: Scotland; EG: England, Woods et al., 2011; S.CN: Southern China, KZ: Kazakhstan, Saltzman et al., 2000; SB: Siberia, Kouchinsky et al., 2008; UT: Utah, MN: Minnesota, IA: Iowa, NF: Newfoundland, AS: Australia, NV: Nevada, Saltzman et al., 2011; SD: Sweden (Baltica), Zhao et al., 2023; N. CN: Northern China, Zhang et al., 2022).

5.6 Comparative analysis of global SPICE events

As a well-documented anoxic event at the Late Cambrian, the SPICE event possessed a rich database, offering valuable insights into the evolution of redox trends during the Late Cambrian. The occurrence of the SPICE event is not geographically restricted and can be observed in various marine environments such as lagoons, platforms, platform edges, slopes, basin margins, and deep basins (Schiffbauer et al., 2017). Within the research concerning the redox conditions of the SPICE events, some cases illustrated localized and brief euxinia in water columns (LeRoy et al., 2021), while others described extensive and prolonged euxinia (Gill et al., 2011). Therefore, this study aims to summarize trends in Late Cambrian redox evolution by contrasting the redox conditions of SPICE events worldwide.

To classify the sedimentary depths of global SPICE events, tidal flats, lagoons, and inner shelves are categorized as shallow-water settings, while outer shelves and shelf edges are defined as intermediate depths. Slopes and deep basins are classified as deep-sea environments. Following this, a comprehensive survey of global instances which had dependable redox proxies to discriminate between oxic, suboxic, anoxic, and euxinic conditions was compiled (Table 3).

Table 3 Comparative analysis of global SPICE event sedimentary environments and redox fluctuations.

Depth	Location	Sedimentary environment	Redox condition	Data source
Shallow	Durness, Scotland	Tidal flat	Suboxia to anoxia with potential euxinia	
	Nuneaton, England	Inner shelf	Anoxia with transient euxinia	LeRoy et al., 2021
	South Korea	Shallow carbonate platform	Anoxia with brief oxic intervals	Choi et al., 2016; LeRoy et al., 2021
	South China	Shallow carbonate platform	Oxygenation with suboxic intervals	Zhang et al., 2023
	North Chian	Shallow carbonate platform	Dysoxia to anoxia	Zhang et al., 2022
Intermediate	Queensland Australia	Outer shelf (below wave base)	Euxinia with subsequent anoxia (ferruginous)	Dhal et al., 2014
Deep	South Sweden	Sloping shelf (below storm wave base)	Euxinia with short oxygenation	Gill et al., 2011
	South Sweden	Epicontinental sea (below storm wave base)	Euxinia with sparse ferruginous intervals	Gill et al., 2021
	South Sweden	Epicontinental sea (below storm wave base)	Euxinic expansion with subsequent contraction	Zhao et al., 2023

A conspicuous pattern emerged within the SPICE event: euxinia predominantly occurred in intermediate to deep environments, while oxidation to anoxia prevailed in shallow columns, with no anoxic record in the early stage. This observation underscored the prevalence of

euxinic water columns in the deep ocean during the Late Cambrian (Gill et al., 2011). Despite variations in the peak of SPICE events, there was a widespread consensus that it typically initiated during transgression (Saltman et al., 2004; Woods et al., 2011; Raine and Smith, 2012, 2017; Schiffbauer et al., 2017). Rising sea levels facilitated the upwelling of deep-sea euxinic water columns, expanding euxinia into shallow continental shelves with relatively oxygen-rich environments, resulting in the coexistence of oxic euxinic and ferruginous zones (Li et al., 2010). This served as a direct mechanism for biotic extinctions within shallow-water continental shelf zones or as an indirect mechanism, such as through the loss of well-oxygenated shelf territories, increasing competition in the remaining habitable areas (LeRoy et al., 2021). Additionally, data on Fe speciation from inner shelf areas suggested that oxygen consumption intensified during and following the SPICE event, leading to instances of anoxia and, in some cases, euxinia (Cuggy, 1996; Gerhardt and Gill, 2016; LeRoy and Gill, 2019). The Durness SPICE event exemplified this phenomenon.

Lower diversity and deeper marine, as SPICE events observed in successions of Baltica and Avalonia, experienced significantly reduced turnovers (Woods et al., 2011). The morphological characteristics of the trilobites and other organisms comprising this assemblage suggest their adaptations to the low oxygen conditions, as evidenced by their presence near the oxygenated edge of the chemocline adjacent to anoxic conditions in deep-water columns. (Clarkson and Taylor, 1995; Clarkson, 2011; Fortey, 2000, Fortey, 1985; Fortey and Wilmot, 1991; Williams et al., 2011)

Furthermore, as the anoxic zones expanded on the shallow continental shelf, the oxygen-depleted bottom water layers also enlarged. Deep-sea organisms adapted to these low-oxygen environments would be capable of settling in continental shelf regions covered by these conditions, replacing the extinct or struggling shallow-water benthic communities that could not survive due to their greater oxygen requirements. After the extinction event,

with increased oxygen utilization in these shelf environments, the fauna could re-diversify, occupying available ecological niches, until eventually, the oxygen-depleted waters once again inundated the shelf, repeating the process (Fortey, 1989; Loch et al., 1993; Palmer, 1984).

Moreover, unstable redox environments in the Early Paleozoic not only drove species extinctions but also played a critical role in driving evolutionary innovations (Wood and Erwin, 2018). The unique evolutionary dynamics of the Early Paleozoic were inherently linked to the nature of marine redox conditions and perturbations in marine spatiotemporal structure. The data provided by these SPICE events supported the view that deep-sea anoxia and its expansion onto shallow marine shelves may have served as environmental drivers for the high extinction rates and origination during the Middle-Late Cambrian and Early Ordovician. It was only when the frequency and intensity of these shallow anoxic events diminished into the Ordovician that a more stable nearshore environment was established, ultimately promoting the rapid and sustained diversification seen in the Great Ordovician Biodiversification Event (Saltzman et al., 2015).

5.7 The palaeontological record of the SPICE event

5.7.1 The trilobite mass extinction

Although it is challenging to preserve fossil traces within the dolomite formations, there is no doubt that the onset of the SPICE event corresponded to the trilobite (*Glyptagnostus stolidotus*) mass extinction (Section 1.5). This study suggested a connection between the rising sea level and the trilobite extinction. While the expansion of euxinic water columns onto shallow continental shelves could result in biotic extinctions (Arthur et al., 1987), the Durness SPICE event aligned with a brief oxygenated phase resulting from increased ocean productivity. Furthermore, during the initial stages of SPICE events on shallow continental shelves, severe anoxia was not prevalent (LeRoy et al., 2021; Zhang et al.,

2023; Zhang et al., 2022). Therefore, the upwelling of euxinic water should not be considered the direct cause of the *Glyptagnostus reticulatus* extinction, although it holds the potential to drive the extinction of *irvingelle*, marking the culmination of the SPICE event. The first appearance of *Glyptagnostus reticulatus* coincided with the onset of sea-level rise (Fan et al., 2011), so the trilobite extinction is more likely attributed to the increase in primary ocean productivity, leading to nutrient depletion and food chain disruption (Saltzman et al., 2000). This scenario has been documented (Paul and Mitchell, 1994).

Another possible trigger is the cooling of shallow seawater. Some studies have proposed that throughout the entire Cambrian, a persistent thermocline separated warm, provincial platform trilobite assemblages from the cold-water cosmopolitan trilobites (Babcock, 1994; Cook and Taylor, 1975). The latter were capable of colonizing shallow, high-latitude, epicontinental seas in Avalonia and the Baltic region but were also found to invade tropical continental shelves during high sea-level phases. Hence, it is evident that cold-water trilobites could migrate globally beneath the thermocline (Saltzman et al., 2000). Stitt (1975) and Palmer (1984) implied that the extinction of warm, regional trilobite assemblages during the Steptoean was a consequence of oceanic turnover-induced cooling. Oxygen isotope data recorded in brachiopod apatite of inarticulate brachiopods samples by Elrick et al. (2011) indicated a significant increase during the early stages of the SPICE event, coinciding with the trilobite mass extinction. This supported the hypothesis of cold-water upwelling onto shallow continental shelves. The cooling of shallow-water platforms allowed trilobite communities typically inhabiting cool deep-sea environments to replace those in the warm shallow-water faunas.

Similarly, a noticeable elevation in oxygen isotope was observed during the early stages of the Durness SPICE event (Fig. 15), potentially lending support to this view. Although diagenesis can readily alter the oxygen isotope records of carbonate rocks (Feng et al.,

2021), Durness dolomites exhibit penecontemporaneous sabkha dolomitization, characterized by a relatively low degree of diagenetic alteration, which allows for the preservation of primary oxygen isotopes. Moreover, the oxygen isotope characteristics of Durness dolomites closely resemble those of apatitic inarticulate brachiopods from Elrick et al. (2011), further substantiating this (typically, the dolomitization exerts a more conservative influence on carbon isotopes, Schiffbauer et al., 2017). Nevertheless, Pratt, 1992 and 1998 documented a sub-Steptoean mass extinction of local trilobites in deep-slope environments, thus, confirming that deep cold-water upwelling is likely not the primary cause of the trilobite mass extinction (although it may have indeed occurred) (Saltzman et al., 2000). Further research with more cases that retain the original temperatures of the SPICE event is required to investigate this potential driving force behind the trilobite mass extinction.

5.7.2 The Great Ordovician Biodiversification Event

From the late Cambrian through much of the Ordovician, a series of complex and diachronous phases of diversification in planktonic organisms and animals are collectively referred to as the Great Ordovician Biodiversification Event (GOBE) or the Ordovician Radiation (Webby et al., 2004; Servais et al., 2010; Miller and Foote, 1996). During the SPICE event, repeated increases in the availability of marine nutrients would have fostered diverse phytoplankton populations across various marine habitats, potentially enhancing both phytoplankton diversity and the diversity of heterotrophic organisms that depended on them as a food source (Dahl et al., 2014). This post-SPICE increase in phytoplankton biodiversity has been documented by Servais et al., 2008. Though there was a slight decrease in the diversity of Phanerozoic marine organisms during the late Cambrian anoxic period, explosive growth occurred during the Ordovician (Fig. 26). The early Paleozoic radiation of phytoplankton paralleled the prolonged rise in sea levels from the Early Cambrian to the Late Ordovician. In the late Cambrian, following the SPICE event, significant changes in morphological disparity and taxonomic diversity occurred in

acritarchs during the Middle Ordovician (Darriwilian), reaching their peak (Servais et al., 2008). However, a significant time lag existed between the SPICE event and the diversification of phytoplankton in the Middle Ordovician. The two most widely accepted diversity pulses of the GOBE occurred approximately 25 million and 35 million years after the SPICE event (Droser and Sheehan, 1997; Droser and Finnegan, 2003; Trotter et al., 2008; Saltzman et al., 2011). This notable time delay demands elucidation.

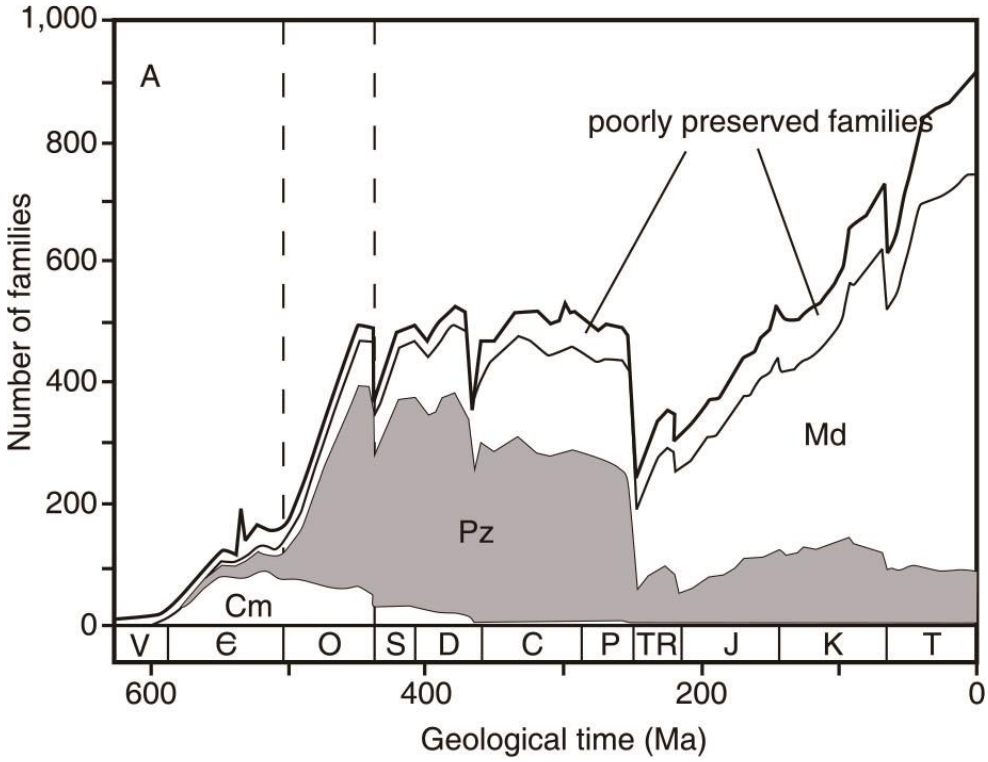

Fig. 26 Phanerozoic marine biodiversity (modified after Sepkoski 1984). Cm: Cambrian evolutionary fauna; Pz: Paleozoic evolutionary fauna; Md: Modern evolutionary fauna.

The atmospheric O_2 is determined by the balance between oxygen produced through photosynthesis and oxygen consumed through the decomposition of dead plants and algae. When the decomposition of organic matter slows down or ceases, the atmospheric O_2 increases. Particularly in ferruginous settings, the particulates of Fe (oxyhydr) oxides combine with deceased organisms, facilitating the preservation of organic matter, which can lead to orders of magnitude increase in atmospheric O_2 (Zhao et al., 2023a) (Fig. 27). The Fe_{py}/Fe_{HR} ratios indicated the presence of distinct ferruginous conditions in the

Durness SPICE event, which is also observed in other shallow-water SPICE events (LeRoy et al., 2021). This widespread prevalence of ferruginous environments can substantially enhance atmospheric oxygen content, and such an increase following SPICE events has been documented (Saltzman et al., 2011).

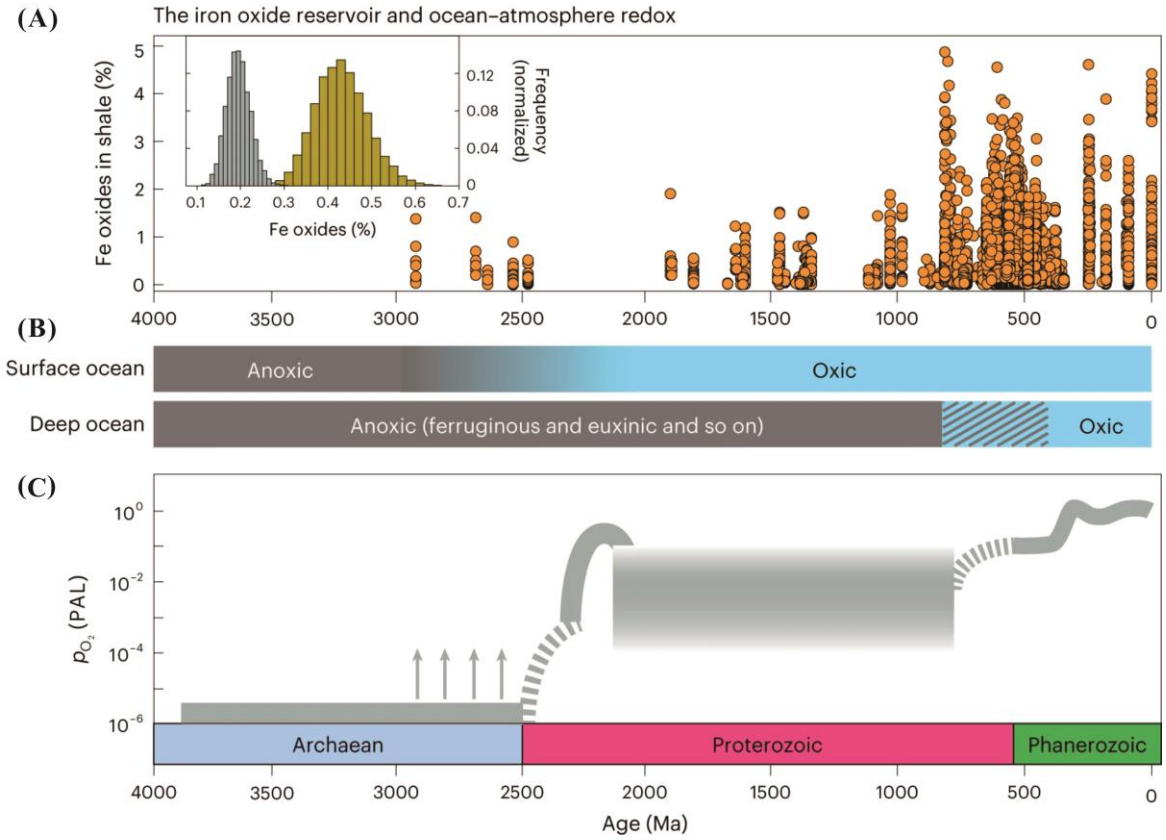

Fig. 27 (A) The evolution of Fe (oxyhydr) oxides concentrations in shale over time. The panel in the upper left illustrates the frequency distribution of bootstrap resampled mean concentrations of Fe (oxyhydr) oxides in shale before 830 Ma (depicted in grey) and after 830 Ma (represented in yellow) (n = 10,000); (B) The approximate trend of marine redox evolution over time; (C) The current comprehension of the evolution of atmospheric pO_2 relative to contemporary atmospheric levels (PAL) (modified after Zhao et al., 2023a).

Saltzman et al. (2011) calculated through isotope mass balance models of $\delta^{13}C$ and $\delta^{34}S$ and proved that atmospheric pO_2 rose from 10 ~ 20 atm% to 10 ~ 30 My after the SPICE event and remained elevated in the atmosphere for tens of millions of years, while the gradually oxidizing deep oceans led to the eventual cessation of recurring "biomere" extinction events. Regardless of the specifics, the O_2 pulse during the Late Cambrian SPICE event played a crucial role in biological evolution, persisting into the Ordovician.

Based on the recent compilations of global or regional marine animal diversity (Sepkoski, 1997; Rong et al., 2007; Alroy, 2010), the GOBE can be considered to have its origins firmly rooted in the Late Cambrian (Furongian). Therefore, the sustained rise in atmospheric O_2 altered the post-SPICE oceanic redox conditions and the concentration of bioavailable nutrients in the surface oceans, ultimately fostering diversification in certain phytoplankton communities and potentially enhancing overall net primary productivity (Saltzman et al., 2011). In sum, the SPICE event laid the necessary foundation for the GOBE.

6. Conclusion

This study employed comprehensive sedimentological and geochemical analysis for the Durness SPICE event, in conjunction with a global SPICE event comparative perspective to elucidate the processes and driving forces of the SPICE event, and its profound significance for the trilobite mass extinction and the Late Cambrian to Ordovician biotic evolution.

The SPICE event corresponded with the transgressive-regressive cycles of the Sauk Megasequence. During the initial phase of rising sea level, the upwelling of nutrient-rich deep seawater enhanced marine primary productivity, leading to the extensive proliferation and subsequent decomposition of phytoplankton. This intensified oceanic oxygen consumption, and led to suboxic (ferruginous) conditions, subsequently raising carbon isotopes, thereby triggering the SPICE event. After a period of relatively high sea level, carbon isotopes gradually reverted towards the baseline. Subsequently, during the rapid regression at the Sauk II-III Supersequence Boundary, intensified continental weathering once again introduced additional nutrients and increased carbon isotope. This further depleted oxygen in seawater, shifting it from suboxic to anoxic (ferruginous) environments. In the transgressive phase of Sauk III, potential localized euxinia occurred. Global redox comparisons of SPICE events demonstrate a trend of extensive deep euxinic environments expanding towards shallow continental shelves. Furthermore, latitude appears to be a primary controlling factor for the location of the SPICE peak, with it becoming more pronounced around the Sauk II-III Supersequence Boundary in regions closer to the equator. Additionally, Fe speciation exhibited excellent redox-indicative behavior in carbonate samples with iron content exceeding 0.5 wt%.

The trilobite mass extinction at the base of the SPICE event was not attributed to the extension of deep euxinia, and the theory of upwelling of cold deep seawater has been

refuted. The disruption of the food chain due to the consumption of essential nutrients resulting from increased marine primary productivity emerges as a plausible driver for the trilobite mass extinction.

A post-SPICE rise in atmospheric oxygen levels has been observed, and the uncertainty regarding the mechanism behind this rise can be elucidated by the widespread ferruginous conditions during the SPICE event. Abundant particulates of Fe (oxyhydr) oxides in ferruginous environments can significantly enhance atmospheric oxygen levels, laying a critical foundation for the subsequent Great Ordovician Biodiversification Event that occurred 30-40 million years later.

In summary, as a globally significant Late Cambrian anoxic event, the SPICE recorded within the Durness Group represents a localized sedimentary condition. Variations in water depth, platform geometry, local biological productivity, and hydrochemistry can influence the way these rock records were preserved. However, the comprehensive insights provided in this study into eustatic changes and redox fluctuations, as well as the implications for biotic evolution, encompassing the collaborative controls of deep nutrient-rich upwelling and intensified continental weathering on the SPICE event, the diverse local expressions of the SPICE event on a global scale, a more rational explanation for the trilobite mass extinction and a clearer connection between the SPICE event and the Ordovician radiation, have advanced our understanding of the SPICE event. These contributions can facilitate research on independent SPICE events in other regions or advance research into the broader and more complex processes of the global SPICE event and its impact on the marine carbonate system. Such contributions will help for unraveling the complexity of such a global system.

Acknowledgements

I would like to extend my sincere gratitude to Professor Rachel Wood, my supervisor, for her invaluable guidance and support throughout the entire project. I would also like to express my appreciation to Dr. Fred Bowyer for his assistance in both theoretical knowledge and experimental work. Without their contributions, I would not have been able to complete this dissertation. Furthermore, I wish to acknowledge Mariana Yilales Agelvis for her assistance in the experimental work related to I/(Ca+Mg), as well as the team led by Professor Simon Poulton at the University of Leeds, particularly Dr. Yijun Xiong, for their guidance and support in the analysis of Fe speciation and total digestion. The Cohen Geochemistry Laboratory at the University of Leeds has provided me with valuable insights into experimental principles and protocols, for which I am truly grateful.

Additionally, I would like to express my thanks to the MScR palaeontology and Geobiology cohort. It has been a delightful and supportive academic family, and I really cherish the enjoyable journey at the University of Edinburgh.

References

Adelson, J. M., Helz, G. R., & Miller, C. V. (2001). Reconstructing the rise of recent coastal anoxia; molybdenum in Chesapeake Bay sediments. *Geochimica et Cosmochimica Acta*, *65*(2), 237-252.

Algeo, T. J., & Maynard, J. B. (2004). Trace-element behaviour and redox facies in core shales of Upper Pennsylvanian Kansas-type cyclothems. *Chemical geology*, *206*(3-4), 289-318.

Algeo, T. J., & Tribovillard, N. (2009). Environmental analysis of paleoceanographic systems based on molybdenum–uranium covariation. *Chemical Geology*, *268*(3-4), 211-225.

Alroy, J. (2010). The shifting balance of diversity among major marine animal groups. *Science*, *329*(5996), 1191-1194.

Anderson, R. F., Fleisher, M. Q., & LeHuray, A. P. (1989). Concentration, oxidation state, and particulate flux of uranium in the Black Sea. *Geochimica et Cosmochimica Acta*, *53*(9), 2215-2224.

Anderson, T. F., & Raiswell, R. (2004). Sources and mechanisms for the enrichment of highly reactive iron in euxinic Black Sea sediments. *American Journal of Science*, *304*(3), 203-233.

Arthur, M. A., Schlanger, S. T., & Jenkyns, H. C. (1987). The Cenomanian-Turonian Oceanic Anoxic Event, II. Palaeoceanographic controls on organic-matter production and preservation. *Geological Society, London, Special Publications*, *26*(1), 401-420.

Babcock, L. E. (1994). Biogeography and biofacies patterns of Middle Cambrian polymeroid trilobites from North Greenland: palaeogeographic and palaeo-oceanographic implications. *Bulletin Grønlands Geologiske Undersøgelse*, *169*, 129-147.

Beerling, D. J., Lake, J. A., Berner, R. A., Hickey, L. J., Taylor, D. W., & Royer, D. L. (2002). Carbon isotope evidence implying high O2/CO2 ratios in the Permo-Carboniferous atmosphere. *Geochimica et Cosmochimica Acta*, *66*(21), 3757-3767.

Berner, R. A. (2001). Modeling atmospheric O2 over Phanerozoic time. *Geochimica et Cosmochimica Acta*, *65*(5), 685-694.

Berner, R. A. (2003). The long-term carbon cycle, fossil fuels and atmospheric composition. *Nature*, *426*(6964), 323-326.

Berner, R. A. (2006). GEOCARBSULF: a combined model for Phanerozoic atmospheric O2 and CO2. *Geochimica et Cosmochimica Acta*, *70*(23), 5653-5664.

Berrang, P. G., & Grill, E. V. (1974). The effect of manganese oxide scavenging on molybdenum in Saanich Inlet, British Columbia. *Marine Chemistry*, *2*(2), 125-148.

Bertine, K. K., & Turekian, K. K. (1973). Molybdenum in marine deposits. *Geochimica et Cosmochimica Acta*, *37*(6), 1415-1434.

Bowyer, F. T. (2018). *Triggering the Cambrian Explosion: carbon cycle reorganisation and the rise*

of Metazoans (Doctoral dissertation, University of Edinburgh).

Böning, P., Brumsack, H. J., Böttcher, M. E., Schnetger, B., Kriete, C., Kallmeyer, J., & Borchers, S. L. (2004). Geochemistry of Peruvian near-surface sediments. *Geochimica et cosmochimica acta*, *68*(21), 4429-4451.

Brasier, M. D., Corfield, R. M., Derry, L. A., Rozanov, A. Y., & Zhuravlev, A. Y. (1994). Multiple δ13C excursions spanning the Cambrian explosion to the Botomian crisis in Siberia. *Geology*, *22*(5), 455-458.

Breit, G. N., & Wanty, R. B. (1991). Vanadium accumulation in carbonaceous rocks: a review of geochemical controls during deposition and diagenesis. *Chemical Geology*, *91*(2), 83-97.

Broecker, W. S., & Peng, T. H. (1982). *Tracers in the Sea* (Vol. 690). Palisades, New York: Lamont-Doherty Geological Observatory, Columbia University.

Brumsack, H. J. (1989). Geochemistry of recent TOC-rich sediments from the Gulf of California and the Black Sea. *Geologische Rundschau*, *78*, 851-882.

Brumsack, H. J. (2006). The trace metal content of recent organic carbon-rich sediments: implications for Cretaceous black shale formation. *Palaeogeography, Palaeoclimatology, Palaeoecology*, *232*(2-4), 344-361.

Calvert, S. E., & Piper, D. Z. (1984). Geochemistry of ferromanganese nodules from DOMES Site A, Northern Equatorial Pacific: Multiple diagenetic metal sources in the deep sea. *Geochimica et Cosmochimica Acta*, *48*(10), 1913-1928.

Calvent, S. E., & Pedersen, T. (1993). Geochemistry of recent oxic and anoxic sediments: Implications for the geological record. Marine Geology, 113(1/2), 67-88.

Campos, M. L. A. M., Sanders, R., & Jickells, T. (1999). The dissolved iodate and iodide distribution in the South Atlantic from the Weddell Sea to Brazil. *Marine Chemistry*, *65*(3-4), 167-175.

Canfield, D. E., Raiswell, R., Westrich, J. T., Reaves, C. M., & Berner, R. A. (1986). The use of chromium reduction in the analysis of reduced inorganic sulfur in sediments and shales. *Chemical geology*, *54*(1-2), 149-155.

Canfield, D. E., Poulton, S. W., & Narbonne, G. M. (2007). Late-Neoproterozoic deep-ocean oxygenation and the rise of animal life. *Science*, *315*(5808), 92-95.

Canfield, D. E., Poulton, S. W., Knoll, A. H., Narbonne, G. M., Ross, G., Goldberg, T., & Strauss, H. (2008). Ferruginous conditions dominated later Neoproterozoic deep-water chemistry. *Science*, *321*(5891), 949-952.

Cawood, P. A., McCausland, P. J., & Dunning, G. R. (2001). Opening Iapetus: constraints from the Laurentian margin in Newfoundland. *Geological Society of America Bulletin*, *113*(4), 443-453.

Chaillou, G., Anschutz, P., Lavaux, G., Schäfer, J., & Blanc, G. (2002). The distribution of Mo, U, and Cd in relation to major redox species in muddy sediments of the Bay of Biscay. *Marine Chemistry*, *80*(1), 41-59.

Chen, J., Chough, S. K., Han, Z., & Lee, J. H. (2011). An extensive erosion surface of a strongly deformed limestone bed in the Gushan and Chaomidian formations (late Middle Cambrian to Furongian), Shandong Province, China: Sequence–stratigraphic implications. *Sedimentary Geology*, *233*(1-4), 129-149.

Chen, J., Chough, S. K., Lee, J. H., & Han, Z. (2012). Sequence-stratigraphic comparison of the upper Cambrian Series 3 to Furongian succession between the Shandong region, China and the Taebaek area, Korea: high variability of bounding surfaces in an epeiric platform. *Geosciences Journal*, *16*, 357-379.

Chester, R., 2000. *Marine Geochemistry*. Blackwell, London. 506 pp.

Choi, D. K., Lee, J. G., LEE, S. B., PARK, T. Y. S., & Hong, P. S. (2016). Trilobite biostratigraphy of the lower Paleozoic (Cambrian–Ordovician) Joseon Supergroup, Taebaeksan Basin, Korea. *Acta Geologica Sinica-English Edition*, *90*(6), 1976-1999.

Clarkson, E. N., & Taylor, C. M. (1995). The lost world of the olenid trilobites. *Geology Today*, *11*(4), 147-154.

Clarkson, E. N. (2011). The life and times of the olenid trilobites. *Geologické výzkumy na Moravě a ve Slezsku*, *18*(1).

Clarkson, M. O., Poulton, S. W., Guilbaud, R., & Wood, R. A. (2014). Assessing the utility of Fe/Al and Fe-speciation to record water column redox conditions in carbonate-rich sediments. *Chemical Geology*, *382*, 111-122.

Cocks, L. R. M., & Torsvik, T. H. (2006). European geography in a global context from the Vendian to the end of the Palaeozoic. *In:* GEE, D.G. & STEPHENSON, R.A. (eds). *European Lithosphere Dynamics*. Geological Society, London, Memoirs, **32**, 83–95.

Cocks, L. R. M., & Torsvik, T. H. (2011). The Palaeozoic geography of Laurentia and western Laurussia: a stable craton with mobile margins. *Earth-Science Reviews*, *106*(1-2), 1-51.

Cole, D. B., Zhang, S., & Planavsky, N. J. (2017). A new estimate of detrital redox-sensitive metal concentrations and variability in fluxes to marine sediments. *Geochimica et Cosmochimica Acta*, *215*, 337-353.

Cowan, C. A., Runkel, A. C., & Saltzman, M. R. (2003, November). The effect on paleoproductivity of the first major delivery of mid Laurentian saprolite-derived material to Phanerozoic oceans: continent-wide marine ravinement during submergence–emergence of Late Cambrian North America, and the global carbon isotope SPICE event. In *Geological Society of America, Abstracts with Programs* (Vol. 35, p. 458).

Cowie, J. W., AWA, R., & CJ, S. (1972). *A correlation of Cambrian rocks in the British Isles*. Geological Society of London Special Report, 2, 42 pp.

Crusius, J., Calvert, S., Pedersen, T., & Sage, D. (1996). Rhenium and molybdenum enrichments in sediments as indicators of oxic, suboxic and sulfidic conditions of deposition. *Earth and Planetary Science Letters*, *145*(1-4), 65-78.

Cuggy, M. B. (1996). Patterns of faunal change at an upper Cambrian trilobite extinction event, Nolichucky Formation, Tennessee and Virginia.

Cutter, G. A., Moffett, J. W., Nielsdóttir, M. C., & Sanial, V. (2018). Multiple oxidation state trace elements in suboxic waters off Peru: In situ redox processes and advective/diffusive horizontal transport. *Marine Chemistry*, *201*, 77-89.

Deng, H., & Qian, K. (1993). Sedimentary Geochemistry and Environmental Analysis. Gansu Science and Technology Press, Lanzhou.

Dickson, J. A. D. (1965). A modified staining technique for carbonates in thin section. *Nature*, *205*(4971), 587-587.

Dong, Z. G., Zhang, L. C., Wang, C. L., Zhang, B. L., Peng, Z. D., Zhu, M. T., ... & Xie, Y. Q. (2020). Progress and problems in understanding sedimentary manganese carbonate metallogenesis. *Miner. Depos*, *39*, 237-255.

Droser, M. L., & Sheehan, P. M. (1997). Palaeoecology of the ordovicianradiation; resolution of large-scale patterns with individual clade histories, palaeogeography and environments. *Geobios*, *30*, 221-229.

Droser, M. L., & Finnegan, S. (2003). The Ordovician radiation: a follow-up to the Cambrian explosion?. *Integrative and Comparative Biology*, *43*(1), 178-184.

Edwards, C. T., Fike, D. A., Saltzman, M. R., Lu, W., & Lu, Z. (2018). Evidence for local and global redox conditions at an Early Ordovician (Tremadocian) mass extinction. *Earth and Planetary Science Letters*, *481*, 125-135.

Elrick, M., Rieboldt, S., Saltzman, M., & McKay, R. M. (2011). Oxygen-isotope trends and seawater temperature changes across the Late Cambrian Steptoean positive carbon-isotope excursion (SPICE event). *Geology*, *39*(10), 987-990.

Emerson, S. R., & Huested, S. S. (1991). Ocean anoxia and the concentrations of molybdenum and vanadium in seawater. *Marine Chemistry*, *34*(3-4), 177-196.

Erickson, B. E., & Helz, G. R. (2000). Molybdenum (VI) speciation in sulfidic waters:: stability and lability of thiomolybdates. *Geochimica et Cosmochimica Acta*, *64*(7), 1149-1158.

Faggetter, L. E., Wignall, P. B., Pruss, S. B., Sun, Y., Raine, R. J., Newton, R. J., ... & Smith, P. M. (2018). Sequence stratigraphy, chemostratigraphy and facies analysis of Cambrian Series 2–Series 3 boundary strata in northwestern Scotland. *Geological Magazine*, *155*(4), 865-877.

Falkowski, P., Scholes, R. J., Boyle, E. E. A., Canadell, J., Canfield, D., Elser, J., ... & Steffen, W. (2000). The global carbon cycle: a test of our knowledge of earth as a system. *science*, *290*(5490), 291-296.

Farrenkopf, A. M., Luther III, G. W., Truesdale, V. W., & Van Der Weijden, C. H. (1997). Sub-surface iodide maxima: evidence for biologically catalyzed redox cycling in Arabian Sea OMZ during the SW intermonsoon. *Deep Sea Research Part II: Topical Studies in Oceanography*, *44*(6-7), 1391-1409.

Farrenkopf, A. M., & Luther Iii, G. W. (2002). Iodine chemistry reflects productivity and denitrification in the Arabian Sea: evidence for flux of dissolved species from sediments of western India into the OMZ. *Deep Sea Research Part II: Topical Studies in Oceanography*, *49*(12), 2303-2318.

Fan, R., Deng, S., & Zhang, X. (2011). Significant carbon isotope excursions in the Cambrian and their implications for global correlations. *Science China Earth Sciences*, *54*, 1686-1695.

Feng, K., Xu, S., Chen, A., Ogg, J., Hou, M., Lin, L., & Chen, H. (2021). Middle Permian dolomites of the SW Sichuan Basin and the role of the Emeishan large igneous province in their origin. *Marine and Petroleum Geology*, *128*, 104981.

Fortey, R. A. (1985). Pelagic trilobites as an example of deducing the life habits of extinct arthropods. *Earth and Environmental Science Transactions of The Royal Society of Edinburgh*, *76*(2-3), 219-230.

Fortey, R. A. (1989). There are extinctions and extinctions: examples from the Lower Palaeozoic. *Philosophical Transactions of the Royal Society of London. B, Biological Sciences*, *325*(1228), 327-355.

Fortey, R. A., & Wilmot, N. V. (1991). Trilobite cuticle thickness in relation to palaeoenvironment. *Paläontologische Zeitschrift*, *65*(1-2), 141-151.

Fortey, R. (2000). Olenid trilobites: The oldest known chemoautotrophic symbionts? *Proceedings of the National Academy of Sciences*, *97*(12), 6574-6578.

Fossing, H., & Jørgensen, B. B. (1989). Measurement of bacterial sulfate reduction in sediments: evaluation of a single-step chromium reduction method. *Biogeochemistry*, *8*, 205-222.

Froelich, P., Klinkhammer, G. P., Bender, M. A. A., Luedtke, N. A., Heath, G. R., Cullen, D., ... & Maynard, V. (1979). Early oxidation of organic matter in pelagic sediments of the eastern equatorial Atlantic: suboxic diagenesis. *Geochimica et cosmochimica acta*, *43*(7), 1075-1090.

Gerhardt, A. M., & Gill, B. C. (2016). Elucidating the relationship between the later Cambrian end-Marjuman extinctions and SPICE Event. *Palaeogeography, Palaeoclimatology, Palaeoecology*, *461*, 362-373.

Gill, B. C., Lyons, T. W., Young, S. A., Kump, L. R., Knoll, A. H., & Saltzman, M. R. (2011). Geochemical evidence for widespread euxinia in the Later Cambrian ocean. *Nature*, *469*(7328), 80-83.

Gill, B. C., Dahl, T. W., Hammarlund, E. U., LeRoy, M. A., Gordon, G. W., Canfield, D. E., ... & Lyons, T. W. (2021). Redox dynamics of later Cambrian oceans. *Palaeogeography, Palaeoclimatology, Palaeoecology*, *581*, 110623.

Glock, N., Liebetrau, V., & Eisenhauer, A. (2014). I/Ca ratios in benthic foraminifera from the Peruvian oxygen minimum zone: analytical methodology and evaluation as a proxy for redox conditions. *Biogeosciences*, *11*(23), 7077-7095.

Glumac, B., & Walker, K. R. (1998). A Late Cambrian positive carbon-isotope excursion in the

Southern Appalachians; relation to biostratigraphy, sequence stratigraphy, environments of deposition, and diagenesis. *Journal of Sedimentary Research*, *68*(6), 1212-1222.

Goldberg, S., Su, C., & Forster, H. S. (1998). Sorption of Molybdenum on Oxides, Clay Minerals. *Adsorption of metals by geomedia: Variables, mechanisms, and model applications*, 401.

Goldberg, T., Archer, C., Vance, D., Thamdrup, B., McAnena, A., & Poulton, S. W. (2012). Controls on Mo isotope fractionations in a Mn-rich anoxic marine sediment, Gullmar Fjord, Sweden. *Chemical Geology*, *296*, 73-82.

Gould, S. J. (1989). *Wonderful life: the Burgess Shale and the nature of history*. WW Norton & Company.

Hardisty, D. S., Lu, Z., Planavsky, N. J., Bekker, A., Philippot, P., Zhou, X., & Lyons, T. W. (2014). An iodine record of Paleoproterozoic surface ocean oxygenation. *Geology*, *42*(7), 619-622.

Hardisty, D. S., Lu, Z., Bekker, A., Diamond, C. W., Gill, B. C., Jiang, G., ... & Lyons, T. W. (2017). Perspectives on Proterozoic surface ocean redox from iodine contents in ancient and recent carbonate. *Earth and Planetary Science Letters*, *463*, 159-170.

Harper, D. A. (2006). The Ordovician biodiversification: setting an agenda for marine life. *Palaeogeography, Palaeoclimatology, Palaeoecology*, *232*(2-4), 148-166.

Harris, D. C. (2010). *Quantitative chemical analysis*, 6th ed., W. H. Freeman, New York, p. 296.

Hastings, D. W., Emerson, S. R., & Mix, A. C. (1996). Vanadium in foraminiferal calcite as a tracer for changes in the areal extent of reducing sediments. *Paleoceanography*, *11*(6), 665-678.

Helz, G. R., Miller, C. V., Charnock, J. M., Mosselmans, J. F. W., Pattrick, R. A. D., Garner, C. D., & Vaughan, D. J. (1996). Mechanism of molybdenum removal from the sea and its concentration in black shales: EXAFS evidence. *Geochimica et Cosmochimica Acta*, *60*(19), 3631-3642.

Higgins, A. K., Leslie, A. G., & Smith, M. P. (2001). Neoproterozoic–Lower Palaeozoic stratigraphical relationships in the marginal thin-skinned thrust belt of the East Greenland Caledonides: comparisons with the foreland in Scotland. *Geological Magazine*, *138*(2), 143-160.

Hild, E., & Brumsack, H. J. (1998). Major and minor element geochemistry of Lower Aptian sediments from the NW German Basin (core Hohenegglesen KB 40). *cretaceous Research*, *19*(5), 615-633.

Hough, M. L., Shields, G. A., Evins, L. Z., Strauss, H., Henderson, R. A., & Mackenzie, S. (2006). A major sulphur isotope event at c. 510 Ma: a possible anoxia–extinction–volcanism connection during the Early–Middle Cambrian transition? Terra Nova, 18(4), 257-263.

Hu, X., Wang, C., & Li, X. (2001). Stable carbon isotope response to oceanic anoxic events. *Journal of Chengdu Institute of Technology*, *28*(1), 1-6.

Hurtgen, M. T., Pruss, S. B., & Knoll, A. H. (2009). Evaluating the relationship between the carbon

and sulfur cycles in the later Cambrian ocean: an example from the Port au Port Group, western Newfoundland, Canada. *Earth and Planetary Science Letters*, *281*(3-4), 288-297.

Huselbee, M. Y., & Thomas, A. T. (1998). Olenellus and conodonts from the Durness Group, NW Scotland, and the correlation of the Durness succession. *Scottish Journal of Geology*, *34*(1), 83-88.

Jenkyns, H. C. (2010). Geochemistry of oceanic anoxic events. *Geochemistry, Geophysics, Geosystems*, *11*(3).

Johnston, D. T., Poulton, S. W., Dehler, C., Porter, S., Husson, J., Canfield, D. E., & Knoll, A. H. (2010). An emerging picture of Neoproterozoic ocean chemistry: Insights from the Chuar Group, Grand Canyon, USA. *Earth and Planetary Science Letters*, *290*(1-2), 64-73.

Kendall, B., Reinhard, C. T., Lyons, T. W., Kaufman, A. J., Poulton, S. W., & Anbar, A. D. (2010). Pervasive oxygenation along late Archaean ocean margins. *Nature Geoscience*, *3*(9), 647-652.

Kennedy, H. A., & Elderfield, H. (1987a). Iodine diagenesis in pelagic deep-sea sediments. *Geochimica et Cosmochimica Acta*, *51*(9), 2489-2504.

Kennedy, H. A., & Elderfield, H. (1987b). Iodine diagenesis in non-pelagic deep-sea sediments. *Geochimica et Cosmochimica Acta*, *51*(9), 2505-2514.

Klinkhammer, G. P., & Palmer, M. R. (1991). Uranium in the oceans: where it goes and why. *Geochimica et Cosmochimica Acta*, *55*(7), 1799-1806.

Kouchinsky, A., Bengtson, S., Gallet, Y., Korovnikov, I., Pavlov, V., Runnegar, B., ... & Ziegler, K. (2008). The SPICE carbon isotope excursion in Siberia: a combined study of the upper Middle Cambrian–lowermost Ordovician Kulyumbe River section, northwestern Siberian Platform. *Geological Magazine*, *145*(5), 609-622.

Kump, L. R., & Arthur, M. A. (1999). Interpreting carbon-isotope excursions: carbonates and organic matter. *Chemical Geology*, *161*(1-3), 181-198.

Lapworth, C. (1883). VI.—The secret of the highlands. *Geological Magazine*, *10*(3), 120-128.

LeRoy, M. A., & Gill, B. C. (2019). Evidence for the development of local anoxia during the Cambrian SPICE event in eastern North America. *Geobiology*, *17*(4), 381-400.

LeRoy, M. A., Gill, B. C., Sperling, E. A., McKenzie, N. R., & Park, T. Y. S. (2021). Variable redox conditions as an evolutionary driver? A multi-basin comparison of redox in the middle and later Cambrian oceans (Drumian-Paibian). *Palaeogeography, Palaeoclimatology, Palaeoecology*, *566*, 110209.

Li, C., Love, G. D., Lyons, T. W., Fike, D. A., Sessions, A. L., & Chu, X. (2010). A stratified redox model for the Ediacaran ocean. *Science*, *328*(5974), 80-83.

Li, D., Zhang, X., Hu, D., Chen, X., Huang, W., Zhang, X., ... & Shen, Y. (2018). Evidence of a large δ13Ccarb and δ13Corg depth gradient for deep-water anoxia during the late Cambrian SPICE event. *Geology*, *46*(7), 631-634.

Lindsay, J. F., Kruse, P. D., Green, O. R., Hawkins, E., Brasier, M. D., Cartlidge, J., & Corfield, R.

M. (2005). The Neoproterozoic–Cambrian record in Australia: a stable isotope study. *Precambrian Research*, *143*(1-4), 113-133.

Loch, J. D., Stitt, J. H., & Derby, J. R. (1993). Cambrian–Ordovician boundary interval extinctions: implications of revised trilobite and brachiopod data from Mount Wilson, Alberta, Canada. *Journal of Paleontology*, *67*(4), 497-517.

Lu, Z., Jenkyns, H. C., & Rickaby, R. E. (2010). Iodine to calcium ratios in marine carbonate as a paleo-redox proxy during oceanic anoxic events. *Geology*, *38*(12), 1107-1110.

Lu, Z., Hoogakker, B. A., Hillenbrand, C. D., Zhou, X., Thomas, E., Gutchess, K. M., ... & Rickaby, R. E. (2016). Oxygen depletion recorded in upper waters of the glacial Southern Ocean. *Nature communications*, *7*(1), 11146.

Lu, W., Wörndle, S., Halverson, G. P., Zhou, X., Bekker, A., Rainbird, R. H., ... & Lu, Z. (2017). Iodine proxy evidence for increased ocean oxygenation during the Bitter Springs Anomaly. *Geochem. Perspect. Lett*, *5*, 53-57.

Lu, W., Ridgwell, A., Thomas, E., Hardisty, D. S., Luo, G., Algeo, T. J., ... & Lu, Z. (2018). Late inception of a resiliently oxygenated upper ocean. Science, 361(6398), 174-177.

Lu, W., Rickaby, R. E., Hoogakker, B. A., Rathburn, A. E., Burkett, A. M., Dickson, A. J., ... & Lu, Z. (2020). I/Ca in epifaunal benthic foraminifera: A semi-quantitative proxy for bottom water oxygen in a multi-proxy compilation for glacial ocean deoxygenation. *Earth and Planetary Science Letters*, *533*, 116055.

Luther III, G. W., & Campbell, T. (1991). Iodine speciation in the water column of the Black Sea. *Deep Sea Research Part A. Oceanographic Research Papers*, *38*, S875-S882.

Lyons, T. W., & Severmann, S. (2006). A critical look at iron paleoredox proxies: New insights from modern euxinic marine basins. *Geochimica et Cosmochimica Acta*, *70*(23), 5698-5722.

März, C., Poulton, S. W., Beckmann, B., Küster, K., Wagner, T., & Kasten, S. (2008). Redox sensitivity of P cycling during marine black shale formation: dynamics of sulfidic and anoxic, non-sulfidic bottom waters. *Geochimica et Cosmochimica Acta*, *72*(15), 3703-3717.

McLennan, S. M. (2001). Relationships between the trace element composition of sedimentary rocks and upper continental crust. *Geochemistry, Geophysics, Geosystems*, *2*(4).

McManus, J., Berelson, W. M., Klinkhammer, G. P., Hammond, D. E., & Holm, C. (2005). Authigenic uranium: relationship to oxygen penetration depth and organic carbon rain. *Geochimica et Cosmochimica Acta*, *69*(1), 95-108.

Miller, A. I., & Foote, M. (1996). Calibrating the Ordovician radiation of marine life: implications for Phanerozoic diversity trends. *Paleobiology*, *22*(2), 304-309.

Morford, J. L., & Emerson, S. (1999). The geochemistry of redox sensitive trace metals in sediments. *Geochimica et Cosmochimica Acta*, *63*(11-12), 1735-1750.

Morford, J. L., Russell, A. D., & Emerson, S. (2001). Trace metal evidence for changes in the redox environment associated with the transition from terrigenous clay to diatomaceous sediment,

Saanich Inlet, BC. *Marine Geology*, *174*(1-4), 355-369.

Morgan, W. A. (2012). Sequence stratigraphy of the great American carbonate bank.

Murray, J. W. (1975). The interaction of metal ions at the manganese dioxide-solution interface. *Geochimica et Cosmochimica Acta*, *39*(4), 505-519.

Ng, T. W., Yuan, J. L., & Lin, J. P. (2014). The North China Steptoean positive carbon isotope event: new insights towards understanding a global phenomenon. *Geobios*, *47*(6), 371-387.

Och, L. M., & Shields-Zhou, G. A. (2012). The Neoproterozoic oxygenation event: Environmental perturbations and biogeochemical cycling. *Earth-Science Reviews*, *110*(1-4), 26-57.

Olson, S. L., Kump, L. R., & Kasting, J. F. (2013). Quantifying the areal extent and dissolved oxygen concentrations of Archean oxygen oases. *Chemical Geology*, *362*, 35-43.

Palmer, A. R., & Taylor, M. E. (1981). Subdivision of the Sauk sequence. In *Short Papers for the Second International Symposium on the Cambrian System: US Geological Survey, Open-File Report* (pp. 81-743).

Palmer, A. R. (1984). The biomere problem: evolution of an idea. *Journal of Paleontology*, 599-611.

Paul, C. R. C., & Mitchell, S. F. (1994). Is famine a common factor in marine mass extinctions? *Geology*, *22*(8), 679-682.

Paul, K. M., van Helmond, N. A., Slomp, C. P., Jokinen, S. A., Virtasalo, J. J., Filipsson, H. L., & Jilbert, T. (2023). Sedimentary molybdenum and uranium: Improving proxies for deoxygenation in coastal depositional environments. *Chemical Geology*, *615*, 121203.

Peach, B. N., & Horne, J. (1884). Report on the geology of the north-west of Sutherland. *Nature*, *31*(785), 31-35.

Peach, B. N. (1907). *The geological structure of the North-West Highlands of Scotland*. Memoirs of the Geological Survey of Great Britain. 668 pp.

Peng, S., Babcock, L., Robison, R., Lin, H., Rees, M., & Saltzman, M. (2004). Global standard stratotype-section and point (GSSP) of the Furongian Series and Paibian Stage (Cambrian). *Lethaia*, *37*(4), 365-379.

Plint, A. G., & Nummedal, D. (2000). The falling stage systems tract: recognition and importance in sequence stratigraphic analysis. *Geological Society, London, Special Publications*, *172*(1), 1-17.

Post, W. M., Peng, T. H., Emanuel, W. R., King, A. W., Dale, V. H., & DeAngelis, D. L. (1990). The global carbon cycle. *American scientist*, *78*(4), 310-326.

Poulton, S. W., & Raiswell, R. (2002). The low-temperature geochemical cycle of iron: from continental fluxes to marine sediment deposition. *American journal of science*, *302*(9), 774-805.

Poulton, S. W., Fralick, P. W., & Canfield, D. E. (2004). The transition to a sulphidic ocean∼ 1.84 billion years ago. *Nature*, *431*(7005), 173-177.

Poulton, S. W., & Canfield, D. E. (2005). Development of a sequential extraction procedure for iron: implications for iron partitioning in continentally derived particulates. *Chemical geology*, *214*(3-4), 209-221.

Poulton, S. W., Fralick, P. W., & Canfield, D. E. (2010). Spatial variability in oceanic redox structure 1.8 billion years ago. *Nature Geoscience*, *3*(7), 486-490.

Poulton, S. W., & Canfield, D. E. (2011). Ferruginous conditions: a dominant feature of the ocean through Earth's history. *Elements*, *7*(2), 107-112.

Pratt, B. R. (1990). Trilobites of the Marjuman and Steptoean stages (Upper Cambrian), Rabbitkettle Formation, southern Mackenzie Mountains, northwest Canada.

Pratt, B. R. (1998). Probable predation on Upper Cambrian trilobites and its relevance for the extinction of soft-bodied Burgess Shale-type animals. *Lethaia*, *31*(1), 73-88.

Pruss, S. B., Jones, D. S., Fike, D. A., Tosca, N. J., & Wignall, P. B. (2019). Marine anoxia and sedimentary mercury enrichments during the Late Cambrian SPICE event in northern Scotland. *Geology*, *47*(5), 475-478.

Pulsipher, M. A., Schiffbauer, J. D., Jeffrey, M. J., Huntley, J. W., Fike, D. A., & Shelton, K. L. (2021). A meta-analysis of the Steptoean positive carbon isotope excursion: the SPICEraq database. *Earth-Science Reviews*, *212*, 103442.

Raine, R. J. (2010). *The Durness Group of NW Scotland: a stratigraphical and sedimentological study of a Cambro-Ordovician passive margin succession* (Doctoral dissertation, University of Birmingham).

Raine, R. J., & Smith, M. P. (2012). Sequence stratigraphy of the Scottish Laurentian margin and recognition of the Sauk megasequence, 575-596.

Raine, R. J., & Smith, M. P. (2017). Sabkha Facies and the Preservation of A Falling-Stage Systems Tract At the Sauk II–III Supersequence Boundary In the Late Cambrian Eilean Dubh Formation, NW Scotland. *Journal of Sedimentary Research*, *87*(1), 41-65.

Raiswell, R., & Canfield, D. E. (1998). Sources of iron for pyrite formation in marine sediments. *American Journal of Science*, *298*(3), 219-245.

Raiswell, R. (2006). An evaluation of diagenetic recycling as a source of iron for banded iron formations.

Raiswell, R., Tranter, M., Benning, L. G., Siegert, M., De'ath, R., Huybrechts, P., & Payne, T. (2006). Contributions from glacially derived sediment to the global iron (oxyhydr) oxide cycle: Implications for iron delivery to the oceans. *Geochimica et Cosmochimica Acta*, *70*(11), 2765-2780.

Raiswell, R., Hardisty, D. S., Lyons, T. W., Canfield, D. E., Owens, J. D., Planavsky, N. J., ... & Reinhard, C. T. (2018). The iron paleoredox proxies: A guide to the pitfalls, problems and proper practice. *American Journal of Science*, *318*(5), 491-526.

Reinhard, C. T., Planavsky, N. J., Robbins, L. J., Partin, C. A., Gill, B. C., Lalonde, S. V., ... &

Lyons, T. W. (2013). Proterozoic ocean redox and biogeochemical stasis. *Proceedings of the National Academy of Sciences*, *110*(14), 5357-5362.

Reinhard, C. T., Planavsky, N. J., Olson, S. L., Lyons, T. W., & Erwin, D. H. (2016). Earth's oxygen cycle and the evolution of animal life. *Proceedings of the National Academy of Sciences*, *113*(32), 8933-8938.

Reimann, C., & de Caritat, P. (2005). Distinguishing between natural and anthropogenic sources for elements in the environment: regional geochemical surveys versus enrichment factors. *Science of the total environment*, *337*(1-3), 91-107.

Repeta, D. J. (1993). A high resolution historical record of Holocene anoxygenic primary production in the Black Sea. *Geochimica et Cosmochimica Acta*, *57*(17), 4337-4342.

Rong, J. Y., Fang, J. X., Miller, A. I., & Li, G. X. (2007). Dynamic patterns of latest Proterozoic-Palaeozoic-early Mesozoic marine biodiversity in South China. *Geological Journal*, *42*(3-4), 431-454.

Rue, E. L., Smith, G. J., Cutter, G. A., & Bruland, K. W. (1997). The response of trace element redox couples to suboxic conditions in the water column. *Deep Sea Research Part I: Oceanographic Research Papers*, *44*(1), 113-134.

Saltzman, M. R., Runnegar, B., & Lohmann, K. C. (1998). Carbon isotope stratigraphy of Upper Cambrian (Steptoean Stage) sequences of the eastern Great Basin: Record of a global oceanographic event. *Geological Society of America Bulletin*, *110*(3), 285-297.

Saltzman, M. R., Ripperdan, R. L., Brasier, M. D., Lohmann, K. C., Robison, R. A., Chang, W. T., ... & Runnegar, B. (2000). A global carbon isotope excursion (SPICE) during the Late Cambrian: relation to trilobite extinctions, organic-matter burial and sea level. *Palaeogeography, Palaeoclimatology, Palaeoecology*, *162*(3-4), 211-223.

Saltzman, M. R., Cowan, C. A., Runkel, A. C., Runnegar, B., Stewart, M. C., & Palmer, A. R. (2004). The Late Cambrian SPICE ($\delta^{13}C$) event and the Sauk II-Sauk III regression: new evidence from Laurentian basins in Utah, Iowa, and Newfoundland. *Journal of Sedimentary Research*, *74*(3), 366-377.

Saltzman, M. R., Young, S. A., Kump, L. R., Gill, B. C., Lyons, T. W., & Runnegar, B. (2011). Pulse of atmospheric oxygen during the late Cambrian. *Proceedings of the National Academy of Sciences*, *108*(10), 3876-3881.

Saltzman, M. R., Edwards, C. T., Adrain, J. M., & Westrop, S. R. (2015). Persistent oceanic anoxia and elevated extinction rates separate the Cambrian and Ordovician radiations. *Geology*, *43*(9), 807-810.

Sander, R. (2015). Compilation of Henry's law constants (version 4.0) for water as solvent. *Atmospheric Chemistry and Physics*, *15*(8), 4399-4981.

Schiffbauer, J. D., Huntley, J. W., Fike, D. A., Jeffrey, M. J., Gregg, J. M., & Shelton, K. L. (2017). Decoupling biogeochemical records, extinction, and environmental change during the

Cambrian SPICE event. *Science Advances*, *3*(3), e1602158.

Schoepfer, S. D., Shen, J., Wei, H., Tyson, R. V., Ingall, E., & Algeo, T. J. (2015). Total organic carbon, organic phosphorus, and biogenic barium fluxes as proxies for paleomarine productivity. *Earth-Science Reviews*, *149*, 23-52.

Scholz, F., Baum, M., Siebert, C., Eroglu, S., Dale, A. W., Naumann, M., & Sommer, S. (2018). Sedimentary molybdenum cycling in the aftermath of seawater inflow to the intermittently euxinic Gotland Deep, Central Baltic Sea. *Chemical Geology*, *491*, 27-38.

Scotese, C. R. (2009). Late Proterozoic plate tectonics and palaeogeography: a tale of two supercontinents, Rodinia and Pannotia. *Geological Society, London, Special Publications*, *326*(1), 67-83.

Sepkoski, J. J. (1981). A factor analytic description of the Phanerozoic marine fossil record. *Paleobiology*, *7*(1), 36-53.

Sepkoski, J.J. (1984). A kinetic model of Phanerozoic taxonomic diveristy. III. Post-Paleozoic families and mass extinctions. *Paleobiology* 10, 246–267

Sepkoski, J. J. (1997). Biodiversity: past, present, and future. Journal of Paleontology, 71(4), 533-539.

Servais, T., Lehnert, O., Li, J. U. N., Mullins, G. L., Munnecke, A., Nuetzel, A., & Vecoli, M. (2008). The Ordovician Biodiversification: revolution in the oceanic trophic chain. *Lethaia*, *41*(2), 99-109.

Servais, T., Harper, D. A., Munnecke, A., Owen, A. W., & Sheehan, P. M. (2009). Understanding the Great Ordovician Biodiversification Event (GOBE): Influences of paleogeography, paleoclimate, or paleoecology. *GSa Today*, *19*(4), 4-10.

Servais, T., Owen, A. W., Harper, D. A., Kröger, B., & Munnecke, A. (2010). The great Ordovician biodiversification event (GOBE): the palaeoecological dimension. *Palaeogeography, Palaeoclimatology, Palaeoecology*, *294*(3-4), 99-119.

Shang, M., Tang, D., Shi, X., Zhou, L., Zhou, X., Song, H., & Jiang, G. (2019). A pulse of oxygen increase in the early Mesoproterozoic ocean at ca. 1.57–1.56 Ga. *Earth and Planetary Science Letters*, *527*, 115797.

Shimmield, G. B., & Pedersen, T. F. (1990). The geochemistry of reactive trace-metals and halogens in hemipelagic continental-margin sediments. *Reviews in Aquatic Sciences*, *3*(2-3), 255-279.

Sial, A. N., Peralta, S., Ferreira, V. P., Toselli, A. J., Aceñolaza, F. G., Parada, M. A., ... & Pimentel, M. M. (2008). Upper Cambrian carbonate sequences of the Argentine Precordillera and the Steptoean C-Isotope positive excursion (SPICE). *Gondwana Research*, *13*(4), 437-452.

Stitt, J. H. (1975). Adaptive radiation, trilobite paleoecology, and extinction, Ptychaspidid Biomere, Late Cambrian of Oklahoma. In *Evolution and morphology of the Trilobita, Trilobitoidea and Merostomata: Proceedings of the Oslo Meeting, 1973* (pp. 381-390).

Swett, K., & Smit, D. E. (1972). Paleogeography and depositional environments of the Cambro-Ordovician shallow-marine facies of the North Atlantic. *Geological Society of America Bulletin*, *83*(11), 3223-3248.

Taylor, S. R., & McLennan, S. M. (1985). The continental crust: its composition and evolution.

Tobin, K. J., Walker, K. R., Srinivasan, K., & Mark Steinhauff, D. (1996). Suboxic to anoxic diagenesis of platform-marginal ooids and bladed-to-fibrous calcite from the Middle Ordovician Ottosee Formation (east Tennessee). *Geological Society of America Bulletin*, *108*(2), 155-167.

Torsvik, T. H., & Cocks, L. R. M. (2013). Chapter 2 New global palaeogeographical reconstructions for the Early Palaeozoic and their generation. *Geological Society, London, Memoirs*, *38*(1), 5-24.

Torsvik, T. H., Smethurst, M. A., Meert, J. G., Van der Voo, R., McKerrow, W. S., Brasier, M. D., Sturt B.A., & Walderhaug, H. J. (1996). Continental break-up and collision in the Neoproterozoic and Palaeozoic—a tale of Baltica and Laurentia. *Earth-Science Reviews*, *40*(3-4), 229-258.

Tribovillard, N. P., Desprairies, A., Lallier-Vergès, E., Bertrand, P., Moureau, N., Ramdani, A., & Ramanampisoa, L. (1994). Geochemical study of organic-matter rich cycles from the Kimmeridge Clay Formation of Yorkshire (UK): productivity versus anoxia. *Palaeogeography, Palaeoclimatology, Palaeoecology*, *108*(1-2), 165-181.

Tribovillard, N., Riboulleau, A., Lyons, T., & Baudin, F. (2004). Enhanced trapping of molybdenum by sulfurized marine organic matter of marine origin in Mesozoic limestones and shales. *Chemical Geology*, *213*(4), 385-401.

Tribovillard, N., Algeo, T. J., Lyons, T., & Riboulleau, A. (2006). Trace metals as paleoredox and paleoproductivity proxies: an update. *Chemical geology*, *232*(1-2), 12-32.

Trotter, J. A., Williams, I. S., Barnes, C. R., Lécuyer, C., & Nicoll, R. S. (2008). Did cooling oceans trigger Ordovician biodiversification? Evidence from conodont thermometry. *Science*, *321*(5888), 550-554.

Turekian, K. K., & Wedepohl, K. H. (1961). Distribution of the elements in some major units of the earth's crust. *Geological society of America bulletin*, *72*(2), 175-192.

Tyson, R. V., & Pearson, T. H. (1991). Modern and ancient continental shelf anoxia: an overview. *Geological Society, London, Special Publications*, *58*(1), 1-24.

Uahengo, C. I., Shi, X., Jiang, G., & Vatuva, A. (2020). Transient shallow-ocean oxidation associated with the late Ediacaran Nama skeletal fauna: evidence from iodine contents of the Lower Nama Group, southern Namibia. *Precambrian Research*, *343*, 105732.

Van Cappellen, P., & Ingall, E. D. (1994). Benthic phosphorus regeneration, net primary production, and ocean anoxia: A model of the coupled marine biogeochemical cycles of carbon and phosphorus. *Paleoceanography*, *9*(5), 677-692.

Vincent, E., & Berger, W. H. (1985). Carbon dioxide and polar cooling in the Miocene: The Monterey hypothesis. *The carbon cycle and atmospheric CO2: Natural variations Archean to present*, *32*, 455-468.

Vorlicek, T. P., Kahn, M. D., Kasuya, Y., & Helz, G. R. (2004). Capture of molybdenum in pyrite-forming sediments: role of ligand-induced reduction by polysulfides. *Geochimica et Cosmochimica Acta*, *68*(3), 547-556.

Waite, T. J., Truesdale, V. W., & Olafsson, J. (2006). The distribution of dissolved inorganic iodine in the seas around Iceland. *Marine Chemistry*, *101*(1-2), 54-67.

Wang, C., Hu, X., Sarti, M., Scott, R. W., & Li, X. (2005). Upper Cretaceous oceanic red beds in southern Tibet: a major change from anoxic to oxic, deep-sea environments. *Cretaceous Research*, *26*(1), 21-32.

Wanty, R. B., & Goldhaber, M. B. (1992). Thermodynamics and kinetics of reactions involving vanadium in natural systems: Accumulation of vanadium in sedimentary rocks. *Geochimica et Cosmochimica Acta*, *56*(4), 1471-1483.

Webby, B. D., Paris, F., Droser, M. L., & Percival, I. G. (Eds.). (2004). *The great Ordovician biodiversification event*. Columbia University Press.

Wedepohl, K. H. (1991). The composition of the upper earth's crust and the natural cycles of selected metals. Metal in natural raw materials, natural resources. *Metals and their compounds in the environment. Occurrence, analysis and biological relevance*, 3-17.

Wehrli, B., & Stumm, W. (1989). Vanadyl in natural waters: Adsorption and hydrolysis promote oxygenation. *Geochimica et Cosmochimica Acta*, *53*(1), 69-77.

Wei, G., Liu, Y., Li, X., Shao, L., & Liang, X. (2003). Climatic impact on Al, K, Sc and Ti in marine sediments: evidence from ODP Site 1144, South China Sea. *Geochemical Journal*, *37*(5), 593-602.

Wei, H., Wang, X., Shi, X., Jiang, G., Tang, D., Wang, L., & An, Z. (2019). Iodine content of the carbonates from the Doushantuo Formation and shallow ocean redox change on the Ediacaran Yangtze Platform, South China. *Precambrian Research*, *322*, 160-169.

Weissert, H. (1989). C-isotope stratigraphy, a monitor of paleoenvironmental change: a case study from the Early Cretaceous. *Surveys in Geophysics*, *10*(1), 1-61.

Wilde, P., & Berry, W. B. N. (1984). Destabilization of the oceanic density structure and its significance to marine "extinction" events. *Palaeogeography, Palaeoclimatology, Palaeoecology*, *48*(2-4), 143-162.

Williams, M., Vannier, J., Corbari, L., & Massabuau, J. C. (2011). Oxygen as a driver of early arthropod micro-benthos evolution. *PloS one*, *6*(12), e28183.

Wong, G. T., & Brewer, P. G. (1977). The marine chemistry of iodine in anoxic basins. *Geochimica et Cosmochimica Acta*, *41*(1), 151-159.

Wong, G. T., Takayanagi, K., & Todd, J. F. (1985). Dissolved iodine in waters overlying and in the

Orca Basin, Gulf of Mexico. *Marine Chemistry*, *17*(2), 177-183.

Wong, G. T. (1995). Dissolved iodine across the Gulf Stream front and in the South Atlantic Bight. *Deep Sea Research Part I: Oceanographic Research Papers*, *42*(11-12), 2005-2023.

Wood, R. A., Poulton, S. W., Prave, A. R., Hoffmann, K. H., Clarkson, M. O., Guilbaud, R., ... & Kasemann, S. A. (2015). Dynamic redox conditions control late Ediacaran metazoan ecosystems in the Nama Group, Namibia. *Precambrian Research*, *261*, 252-271.

Wood, R., & Erwin, D. H. (2018). Innovation not recovery: dynamic redox promotes metazoan radiations. *Biological Reviews*, *93*(2), 863-873.

Wood, R., Liu, A. G., Bowyer, F., Wilby, P. R., Dunn, F. S., Kenchington, C. G., ... & Penny, A. (2019). Integrated records of environmental change and evolution challenge the Cambrian Explosion. *Nature ecology & evolution*, *3*(4), 528-538.

Wörndle, S., Crockford, P. W., Kunzmann, M., Bui, T. H., & Halverson, G. P. (2019). Linking the Bitter Springs carbon isotope anomaly and early Neoproterozoic oxygenation through I/[Ca+ Mg] ratios. *Chemical Geology*, *524*, 119-135.

Wright, D. T. (1993). *Studies of the Cambrian Eilean Dubh Formation of North-West Scotland* (Doctoral dissertation, University of Oxford).

Wright, D. T., & Knight, I. (1995). A revised chronostratigraphy for the lower Durness Group. *Scottish Journal of Geology*, *31*(1), 11-22.

Xiong, L., Bai, X., Zhao, C., Li, Y., Tan, Q., Luo, G., ... & Song, F. (2022). High-resolution data sets for global carbonate and silicate rock weathering carbon sinks and their change trends. *Earth's Future*, *10*(8), e2022EF002746.

Yang, J., & Xu, S. (2007). Isotopes and Global Environmental Change. Geological Publishing House.

Yuan, C., Liu, S. A., Chen, J., & Fang, L. (2022). Zinc isotopic evidence for enhanced continental weathering and organic carbon burial during the late Cambrian SPICE event. *Palaeogeography, Palaeoclimatology, Palaeoecology*, *608*, 111302.

Zegeye, A., Bonneville, S., Benning, L. G., Sturm, A., Fowle, D. A., Jones, C., ... & Poulton, S. W. (2012). Green rust formation controls nutrient availability in a ferruginous water column. *Geology*, *40*(7), 599-602.

Zeng, N., Qian, H., Munoz, E., & Iacono, R. (2004). How strong is carbon cycle-climate feedback under global warming? *Geophysical Research Letters*, *31*(20).

Zerkle, A. L., Claire, M. W., Domagal-Goldman, S. D., Farquhar, J., & Poulton, S. W. (2012). A bistable organic-rich atmosphere on the Neoarchaean Earth. *Nature Geoscience*, *5*(5), 359-363.

Zhang, L., Algeo, T. J., Zhao, L., Chen, Z. Q., Zhang, Z., & Li, C. (2022). Linkage of the late Cambrian microbe-metazoan transition (MMT) to shallow-marine oxygenation during the SPICE event. *Global and Planetary Change*, *213*, 103798.

Zhang, L., Algeo, T. J., Zhao, L., Dahl, T. W., Chen, Z. Q., Zhang, Z., ... & Li, C. (2023).

Environmental and trilobite diversity changes during the middle-late Cambrian SPICE event. *Geological Society of America Bulletin*.

Zhao, W., & Wan, X. (2003). Late Evolutionary Paleoceanic Events in the Western Tibetan Tethys. Geological Publishing House, Beijing.

Zhao, Z., Thibault, N. R., Dahl, T. W., Schovsbo, N. H., Sørensen, A. L., Rasmussen, C. M., & Nielsen, A. T. (2022). Synchronizing rock clocks in the late Cambrian. *Nature Communications*, *13*(1), 1990.

Zhao, Z., Pang, X., Zou, C., Dickson, A. J., Basu, A., Guo, Z., ... & Dahl, T. W. (2023). Dynamic oceanic redox conditions across the late Cambrian SPICE event constrained by molybdenum and uranium isotopes. *Earth and Planetary Science Letters*, *604*, 118013.

Zhao, M., Mills, B. J., Homoky, W. B., & Peacock, C. L. (2023a). Oxygenation of the Earth aided by mineral–organic carbon preservation. Nature Geoscience, 16(3), 262-267.

Zheng, Y. F. (1999). Oxygen isotope fractionation in carbonate and sulfate minerals. *Geochemical Journal*, *33*(2), 109-126.

Zheng, Y., Anderson, R. F., Van Geen, A., & Kuwabara, J. (2000). Authigenic molybdenum formation in marine sediments: a link to pore water sulfide in the Santa Barbara Basin. *Geochimica et Cosmochimica Acta*, *64*(24), 4165-4178.

Zhou, X., Thomas, E., Rickaby, R. E., Winguth, A. M., & Lu, Z. (2014). I/Ca evidence for upper ocean deoxygenation during the PETM. *Paleoceanography*, *29*(10), 964-975.

Zhou, X., Jenkyns, H. C., Owens, J. D., Junium, C. K., Zheng, X. Y., Sageman, B. B., ... & Lu, Z. (2015). Upper ocean oxygenation dynamics from I/Ca ratios during the Cenomanian-Turonian OAE 2. *Paleoceanography*, *30*(5), 510-526.

Zhu, M. Y., Zhang, J. M., Li, G. X., & Yang, A. H. (2004). Evolution of C isotopes in the Cambrian of China: implications for Cambrian subdivision and trilobite mass extinctions. *Geobios*, *37*(2), 287-301.

Zhu, M. Y., Babcock, L. E., & Peng, S. C. (2006). Advances in Cambrian stratigraphy and paleontology: integrating correlation techniques, paleobiology, taphonomy and paleoenvironmental reconstruction. *Palaeoworld*, *15*(3-4), 217-222.

Zhu, M., Strauss, H., & Shields, G. A. (2007). From snowball earth to the Cambrian bioradiation: calibration of Ediacaran–Cambrian earth history in South China. *Palaeogeography, Palaeoclimatology, Palaeoecology*, *254*(1-2), 1-6.

Zhu, X., Cai, J., Liu, W., & Lu, X. (2016). Occurrence of stable and mobile organic matter in the clay-sized fraction of shale: Significance for petroleum geology and carbon cycle. *International Journal of Coal Geology*, *160*, 1-10.

Zhuravlev, A. Y., & Wood, R. A. (1996). Anoxia as the cause of the mid-Early Cambrian (Botomian) extinction event. *Geology*, *24*(4), 311-314.

Graphical abstract

Mechanisms and Processes of the Durness SPICE Event